AD-A031 299 AIR FORCE GEOPHYSICS LAB HANSCOM AFB MASS F/G 4/2
AREAL COVERAGE ESTIMATES BY STOCHASTIC MODELLING.(U)
JUL 76 I I GRINGORTEN
UNCLASSIFIED AFGL-TR-76-0148 NL

1 OF 1
ADA031299

END

DATE
FILMED
11 -76

AFGL-TR-76-0148
ENVIRONMENTAL RESEARCH PAPERS, NO. 573

Areal Coverage Estimates by Stochastic Modelling

IRVING I. GRINGORTEN

6 July 1976

METEOROLOGY DIVISION PROJECT 8624
AIR FORCE GEOPHYSICS LABORATORY
HANSCOM AFB, MASSACHUSETTS 01731

AIR FORCE SYSTEMS COMMAND, USAF

This technical report has been reviewed and is approved for publication.

FOR THE COMMANDER:

John Howard

Chief Scientist

Qualified requestors may obtain additional copies from the Defense Documentation Center. All others should apply to the National Technical Information Service.

Unclassified

SECURITY CLASSIFICATION OF THIS PAGE (When Data Entered)

REPORT DOCUMENTATION PAGE

READ INSTRUCTIONS BEFORE COMPLETING FORM

(14) 1. REPORT NUMBER: AFGL-TR-76-0148, AFGL-ERP-573

2. GOVT ACCESSION NO.

3. RECIPIENT'S CATALOG NUMBER

(6) 4. TITLE (and Subtitle): AREAL COVERAGE ESTIMATES BY STOCHASTIC MODELLING,

5. TYPE OF REPORT & PERIOD COVERED: Scientific. Interim.

6. PERFORMING ORG. REPORT NUMBER: ERP, No. 573

(10) 7. AUTHOR(s): Irving I. Gringorten

8. CONTRACT OR GRANT NUMBER(s)

9. PERFORMING ORGANIZATION NAME AND ADDRESS
Air Force Geophysics Laboratory (LYK)
L. G. Hanscom AFB
Massachusetts 01731

10. PROGRAM ELEMENT, PROJECT, TASK AREA & WORK UNIT NUMBERS
86240206
62101F

11. CONTROLLING OFFICE NAME AND ADDRESS
Air Force Geophysics Laboratory (LYK)
L. G. Hanscom AFB
Massachusetts 01731

(11) 12. REPORT DATE: 6 July 1976

13. NUMBER OF PAGES: 56

(9) 14. MONITORING AGENCY NAME & ADDRESS (if different from Controlling Office): Environmental research papers

15. SECURITY CLASS. (of this report): Unclassified

15a. DECLASSIFICATION/DOWNGRADING SCHEDULE

16. DISTRIBUTION STATEMENT (of this Report)

Approved for public release; distribution unlimited.

(12) 55p.

17. DISTRIBUTION STATEMENT (of the abstract entered in Block 20, if different from Report)

(16) AF-8624 (17) 862402

18. SUPPLEMENTARY NOTES

19. KEY WORDS (Continue on reverse side if necessary and identify by block number)

Stochastic modelling
Areal extent
Areal coverage
Climatology
Probabilities
Frequency distributions

20. ABSTRACT (Continue on reverse side if necessary and identify by block number)

The purpose of this paper is to relate the single-point probability of a meteorological event to the probability of its occurrence along a line or in an area of given size or fraction of the area. To make the problem tractable it was limited to modelling the probability estimates of the minimum or maximum condition along a line or in an area, or of the maximized minimum in a fraction of the area.

DD FORM 1 JAN 73 1473 EDITION OF 1 NOV 65 IS OBSOLETE

Unclassified

SECURITY CLASSIFICATION OF THIS PAGE (When Data Entered)

409578

AB

20. Abstract (Continued)

In the absence of an analytical solution a Monte Carlo technique, applied to a Gaussian variable, was used to obtain answers that are presented graphically. Two models are described, one shown to be effective with macro-scale events; the other, and more interesting model, is shown to be effective with the mesoscale phenomena of quantitative precipitation in areas ranging from a few hundred square kilometers to more than 50,000 km^2.

SQ. KM.

Preface

The second example of this paper, on New England rainfall, has required data processing by hand. The New England State climatologists, Messrs. Robert Lautzenheiser and Edward Sable, as well as the National Climatic Center's specialists, Harold Crutcher and his associates in Asheville, N.C., were most helpful in locating and providing the data. The statistical processing was the work of student assistants under Sister Leonarda Burke, Regis College, Weston, MA. The third example was initially undertaken, frankly, with doubts as to its feasibility. But the idea was conceived and encouraged by my associates, Messrs. Grantham and Lund, who also undertook much of the preliminary planning. Mr. Grantham instructed the National Climatic Center assistants in Asheville on the data collection. Funds for the radar study were provided by the United States Air Force. The function of the AFCRL Computation Branch's Analysis and Simulation Unit made this study possible through the excellent programming by the contractor, Boston College, on the AFCRL computer installation.

Contents

Illustrations

Tables

Areal Coverage Estimates by Stochastic Modelling

1. INTRODUCTION

At a point of observation, how representative is the weather with respect to the surrounding area? With the passage of a storm, what fraction of a city or state will have received over 25 mm of rainfall, a trace or more, or will have been missed by the storm? What is the probability that a satellite camera will record a clear view of a given area of the globe, or a percentage of the area? These and many more questions on the horizontal persistence or variability in the weather are similar to the questions asked with regard to temporal events. But whereas the latter have been the subject of many successful studies and papers, the problem of areal coverage has remained challenging.

Previous studies of the areal extent of the weather, for the most part, have yielded essentially spatial correlation coefficients, but there have been notable exceptions.. Riedel et al[1] worked with integrated rainfall amounts in areas of given size, making estimates of the maximum possible precipitation falling in periods of 6 to 48 hours. They obtained the variation of extreme total rainfall for areas

(Received for publication 6 July 1976)

1. Riedel, J.F., Appleby, J.F., and Schloemer, R.W. (1956) Seasonal Variation of the Probable Maximum Precipitation East of the 105th Meridian for Areas from 10 to 1000 sq. miles and Durations of 6, 12, 24, and 48 Hours, U.S. Dept. of Commerce, Hydrometeorological Report No. 33, Washington, D.C.

ranging from 26 to 2600 km^2. Among studies of storms, Court[2] reviewed and tested models of rainstorms that were assumed to be symmetrical around a storm center. Likewise the assumption of symmetry was basic to the models of Briggs[3] and Roberts.[4] The latter defined a scale measure, on the order of 80 to 320 km, for the radial extent of precipitation, which he derived from the frequency of the event at a single station and its probability of occurrence somewhere in a dense network of stations.

More recently, Sims and Jones[5] surveyed the rainfall rates averaged over lines 10 to 62 km long in two special field projects, one in central Illinois, the other in Florida. The latter project was part of the well-known 1948 Florida Thunderstorm Project. Sims and Jones' recourse to the data, now more than 25 years old, is indicative of the infrequency of experimental surveys of areal coverage on a mesoscale; however, if experimental efforts have been few, models of areal coverage are virtually nonexistent.

This paper makes no effort to describe, or map, actually occurring details of weather phenomena; rather, its purpose is to estimate the probability of events occurring along lines of travel or within specified areas or fractions thereof. In contrast with Riedel's purpose to present integrated rainfall amounts in a given area, the effort of this paper is centered on the maximum or minimum value of a meteorological element, either in a given area or along a line of travel. The archived data are used, not as comprehensive climatology in themselves, but as a guide to modelling. Additionally, a model is developed to yield answers on the fractional cover of an area.

2. APPROACH

The problem, at the outset, is to devise a procedure that will produce a simulated horizontal synoptic field stochastically, without recourse to physical laws or dynamics. Once this is accomplished, the procedure can be repeated many times to produce a large set of synoptic situations, thus comprising a sample that can be surveyed for spatial correlation or association of events.

---

2. Court, A. (1961) Area-point rainfall formulas, J. Geophys. Res., 66:1823-1831.
3. Briggs, J. (1972) Probability of aircraft encounters with heavy rain, Meteorol. Mag., 101:8-13.
4. Roberts, C. F. (1971) A note of the derivation of a scale measure for precipitation events, Monthly Weather Review, 99:873-876.
5. Sims, A. L. and Jones, D. M. A. (1975) Frequencies of short-period rainfall rates along lines, J. Appl. Meteorol., 14:170-174.

It is assumed that at any single point in the atmosphere the process of change of a weather element is stationary stochastic; that is, it has a partially random pattern of change, and the pattern does not change with time. Further, it is supposed that any meteorological quantity (x) can be transformed into the normalized variable (y) in a one-to-one correspondence. Conventionally the normalized variable is written as y(0, 1) meaning that it has a mean of 0.0 and a variance of 1.0 with the bell-shaped distribution implied. The transformation ($x \rightarrow y$) might be accomplished through algebraic or analytical expressions, but not necessarily. Frequently, it is sufficient to obtain the distribution of y graphically, or tabularly, through the cumulative probability:

$$P(x) = P(y) = 1/\sqrt{2\pi} \int_{-\infty}^{y} \exp(-\xi^2/2)\, d\xi \quad , \tag{1}$$

where the symbol P is used for cumulative probability or the probability that the value in parenthesis is not exceeded.

The transformation ($x \rightarrow y$) is possible for weather elements whether they are continuous, like air temperature, or classified in categories, like sky cover (clear, scattered, broken, or overcast). In one example (Figure 1) the transformation of the Minneapolis January hourly temperature (T) into y(0, 1) is straightforward. The ordinate scale is the cumulative probability P(T) = P(y), and the abscissa is the temperature (T). The value of y(0, 1) is shown alongside P(y), but is available in almost any textbook in statistics. Through the plotted curve (Figure 1) the graphical transformation of T into y(0, 1) is accomplished.

In another example (Table 1) the sky cover in January at midnight in Minneapolis, Minnesota, has been reported in frequencies of 33 percent for clear, 12 percent for scattered clouds, 11 percent for broken clouds, and 44 percent for overcast. From a table of the normal distribution, the variable (y) takes on values: ≤ -0.43 for clear sky, between -0.43 and -0.18 for scattered clouds, between -0.13 and 0.16 for broken clouds, and >0.16 for overcast.

At each station at each time of day in each month or season, an element like temperature will have its own characteristic distribution of values. But all transformed variables (y), from all stations, will have a common distribution with a mean of 0.0, a variance of 1.0, and the Gaussian density function. The goal of this paper is to devise a stochastic process with the normalized variable generated everywhere. Between the values of y at any two stations there will be a correlation that generally will decrease with increasing distance between stations. Within a given area (circle, square, or other shape) there will be a set of values that will have a minimum value and a maximum, also a highest minimum (or lowest

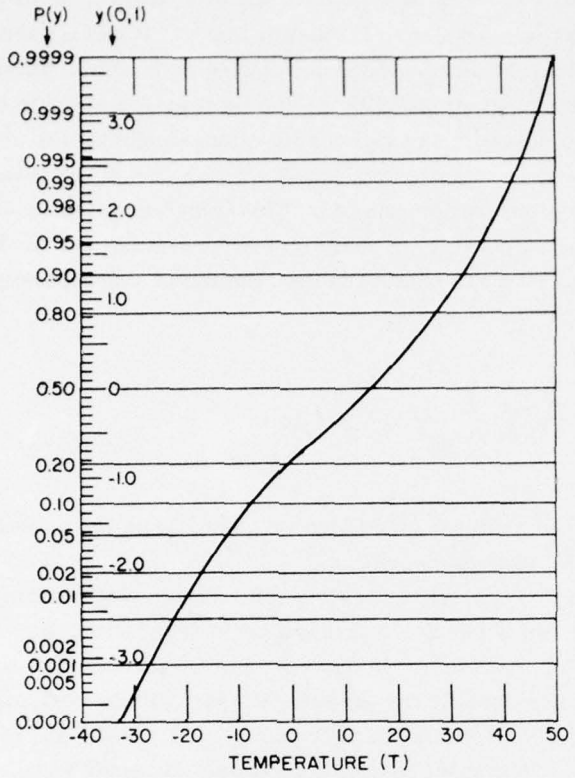

Figure 1. Plot on Normal Probability Paper to Illustrate the Transformation of a Variable (T) into the Normalized Variable y(0, 1) Through the Cumulative Frequency of Values

Table 1. Example of the Transformation of Categories of a Weather Condition Into Intervals of the Normalized Variable (y). The example is for sky cover at Minneapolis, MN., midnight, January

Category Sky Cover	Rel. Freq.	Normalized Variable (y)
Clear	0.33	$y \leq -0.43$
Scattered	0.12	$-0.43 < y \leq -0.13$
Broken	0.11	$-0.13 < y \leq 0.16$
Overcast	0.44	$y > 0.16$

maximum) value for a specified fraction of the area. Each minimum or maximum can be transformed back to the original weather element through reverse application of Eq. (1).

3. SPATIAL CORRELATION

Suppose, initially, random normal numbers (y_o) are assigned to all points of a square grid with a fine mesh (Figure 2). At a given point (i, j) suppose the number $y_o(i, j)$ is replaced with a weighted sum of the surrounding random numbers. If the mesh is infinitesimally fine and the area infinite, then the new number is

$$y(i, j) = \frac{1}{D} \int_{-\infty}^{\infty} \int_{-\infty}^{\infty} F(R) \cdot y_o(i + \xi, j + \eta)\, d\xi\, d\eta \quad , \tag{2}$$

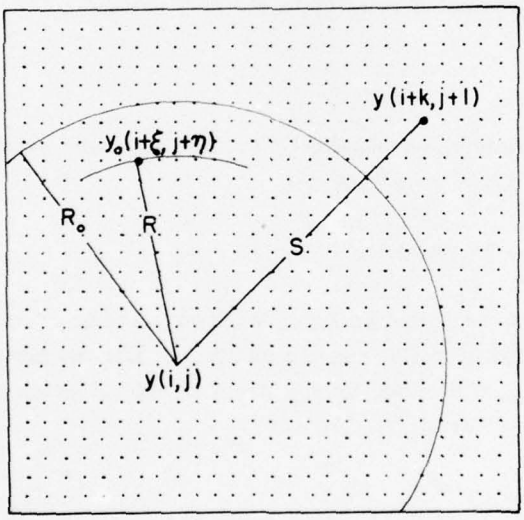

Figure 2. A Grid of Points to Which Random Numbers Are Initially Assigned. The random value $y_o(i + \xi, j + \eta)$ is at distance $R = \sqrt{(\xi^2 + \eta^2)}$ from (i, j). The value y(i, j) is a weighted average of the random numbers surrounding (i, j) within radius R_o. The cc between y(i, j) and $y(i + k, j + \ell)$ decays with the distance $s = \sqrt{(k^2 + \ell^2)}$

where (ξ, η) are coordinates of $(i + \xi, j + \eta)$ relative to (i, j). R is the radial distance, given by

$$R^2 = \xi^2 + \eta^2 \quad . \tag{3}$$

F(R) is the weighting function that generally should decrease with increasing distance (R), and D is a constant, to be determined such that the variance of y(i, j) becomes 1.0.

At another point $(i + k, j + \ell)$, at a distance s from (i, j) given by

$$s^2 = k^2 + \ell^2 \quad , \tag{4}$$

the random number is replaced with

$$y(i + k, j + \ell) = \frac{1}{D} \int_{-\infty}^{\infty} \int_{-\infty}^{\infty} F(R') \cdot y_o(i + k + \xi', j + \ell + \eta') \, d\xi' \, d\eta' \quad , \tag{5}$$

where (ξ', η') are coordinates relative to $(i + k, j + \ell)$ and

$$R'^2 = \xi'^2 + \eta'^2 \quad . \tag{6}$$

The correlation coefficient, hereinafter shortened to cc and symbolized as ρ, between y(i, j) and $y(i + k, j + \ell)$, is

$$\rho(s) = E\{y(i, j) \cdot y(i + k, j + \ell)\} \quad . \tag{7}$$

From (2), (5), (7) it is seen that $\rho(s)$ can be given in terms of an infinite number of the products of pairs of initial random numbers. But the expected product of any two random numbers is zero, unless they coincide in which case their expected product is 1.0. Hence, using (3), (4), (6)

$$\rho(s) = \frac{1}{D^2} \int_{-\infty}^{\infty} \int_{-\infty}^{\infty} F(R) \cdot F(R') \, d\xi \, d\eta \quad , \tag{8}$$

when

$$\xi' = \xi - k \quad , \tag{9}$$

$$\eta' = \eta - \ell \quad .$$

For $s = 0$, $\rho(s) = 1$, hence

$$D^2 = \int_{-\infty}^{\infty} \int_{-\infty}^{\infty} F^2(R)\, d\xi\, d\eta \tag{10}$$

or

$$D^2 = 2\pi \int_{o}^{\infty} R \cdot F(R)\, dR \quad . \tag{11}$$

In practice, for a grid that is less than infinitesimally fine, (2) is approximated by

$$y(i, j) = \frac{1}{D} \sum_{\xi, \eta} F(R) \cdot y_o(i + \xi, j + \eta) \quad , \tag{12}$$

where (ξ, η) are given only in whole units and their vector sum $R \leq R_o$, where R_o is large.

For a finite grid (3) holds for R, (6) for R', and (8) and (10) are approximated by

$$\rho(s) = \frac{1}{D^2} \Sigma F(R) \cdot F(R') \quad , \tag{13}$$

where

$$D^2 = \sum_{\xi, \eta} F^2(R) \quad . \tag{14}$$

If, initially, random numbers (x) with a rectangular distribution between 0.0 and 1.0 are assigned to the grid points, their mean will be 1/2 and variance equal to 1/12. Equation (12) is given alternatively by

$$y(i,\ j) = \left[\Sigma\ F(R) \cdot x_o(i + \xi,\ j + \eta) - 1/2\Sigma\ F(R)\right] \Big/ \sqrt{\Sigma\ F^2(R)/12} \quad . \tag{15}$$

In a Monte Carlo exercise this form of the derivation of y-values from a set of random numbers (x_o) becomes a valuable tool.

So far, the model has been considered in general terms. To proceed further, the form of the weighting function F(R) must be specified. In the following subsections several possibilities are considered, including two of specific interest.

3.1 When Weighting Function Decreases Expontially with Distance

Let the weighting function F(R) be given by

$$F(R) = \exp\ (-R^b/A) \quad , \tag{16}$$

where b is kept within the limits

$$0 < b \leq 2 \quad . \tag{17}$$

The parameter A strengthens or weakens the horizontal persistence. Equation (11) becomes

$$D^2 = m\pi\ (A/2)^m \cdot \Gamma(m) \quad , \tag{18}$$

where $m = 2/b$ and $\Gamma(m)$ is the gamma function of m. For the cc between points separated by s, (8) becomes

$$\rho(s) = \frac{1}{D^2} \int_{-\infty}^{\infty} \int_{-\infty}^{\infty} \exp\left[-(R^b + R'^b)/A\right] d\xi\ d\eta \quad . \tag{19}$$

Except when $b = 2$, attempts at rigorous analysis of (19) failed to produce a simple analytic solution for $\rho(s)$. It was necessary to approximate $\rho(s)$ by numerical process on an electronic computer. This was done, using the Gaussian-Laguerre 24-point double-precision formula[6] with values of b ranging from 0.25 to 1.5. The expertise was provided by Dr. Richard Dougherty, RDP Corporation, Bedford, Massachusetts, serving as a consultant under USAF contract. His

6. Stroud, A. H. and Secrest, D. (1966) Gaussian Quadratic Formulas, Prentice-Hall, Englewood Cliffs, New Jersey.

results showed that the weighting function (16) produces a field in which the cc decreases exponentially as the square of the distance for short distances, then decreases more slowly with increasingly large distances. Such a correlation field does not conform to most previous concepts. For the present the model of (16) has been set aside, except when b = 2, as in the following section.

3.2 Model A: When Weighting Function is Made Proportional to the Bivariate Normal Density Function

Let the weighting function F(R) be given by

$$F(R) = \exp(-R^2/A) \quad , \tag{20}$$

where A again is a parameter that strengthens or weakens the horizontal persistence. Then (11) becomes

$$D^2 = \pi A/2 \tag{21}$$

and (8) resolves and becomes

$$\rho(s) = \exp(-s^2/2A) \quad . \tag{22}$$

Thus, the cc is found to decay exponentially with the square of the distance between stations.

It is convenient to set A = 50, making the cc equal very nearly to 0.99 for unit distance (s = 1).

To conform to previous conceptions, it is desirable to find a field in which the cc decreases exponentially with distance (not squared), at least for short distances. Additionally there would be an advantage to a model in which the cc drops to zero eventually in a large, but finite, distance. This is accomplished in Model B.

3.3 Model B: When the Weight is Made Uniform Within a Circular Area Surrounding the Station

Let the weighing function become simply

$$F(R) = 1 \quad \text{for} \quad R \leq R_o \quad , \tag{23}$$

$$= 0 \quad \text{for} \quad R > R_o \quad ,$$

where R_o is hereafter termed the Radius of Influence (Figure 2). This concept of the weighting function may be resisted at first, but it resembles the concept of the rain cell of Briggs[3] and R_o resembles the "scale measure" of Roberts.[4] The value of y(i, j) at point C_1 or C_2 (Figure 3) is a simple average of many uniformly spaced random numbers inside the circular region of radius R_o that surrounds the point, with a suitable value for D to make the variance of y(i, j) equal to unity. The cc between the two normalized values at C_1 and C_2 is positive only if there is an overlap of the two circles, and is directly proportional to the area of intercept. For the distance s between C_1 and C_2, (8), (11), and (4) yield

$$\rho(s) = \frac{2}{\pi}\left[\sin^{-1}\sqrt{1-\sigma^2} - \sigma\sqrt{1-\sigma^2}\right] \quad \text{for} \quad \sigma < 1 \tag{24}$$

$$= 0 \quad \text{for} \quad \sigma \geq 1 \ ,$$

where

$$\sigma = s/2R_o. \tag{25}$$

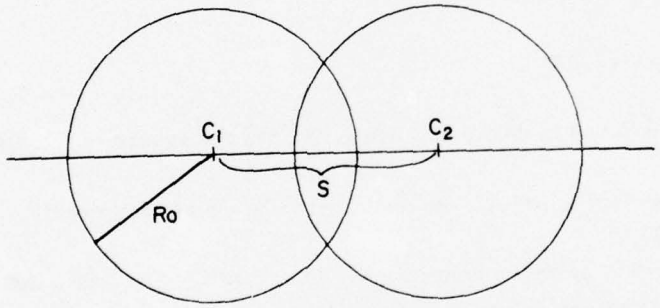

Figure 3. Illustration of the Radius of Influence (R_o). In Model B the intersection of the two circles is a direct measure of the cc between values of a weather element at C_1 and C_2, decreasing with increasing distance (s)

For a small distance s, the Taylor expansion of terms of (24) is approximated by

$$\rho(s) \doteq \exp(-2s/\pi R_o) \ . \tag{26}$$

That is, the cc decreases exponentially with short distances (not squared) between stations. The departure of (24) from (26) is less than 0.1 for $s < 0.8R_o$. But as mentioned in Section 3.2, the decrease of cc to zero at distance $2R_o$ should be an

advantage considering that the cc's reported by most authors do drop to zero at some measurable distance between stations.

It is convenient to set $R_o = 64$ to give the cc, by (24), very nearly equal to 0.99 for a unit distance ($s = 1$).

4. SCALE DISTANCE

In Section 3, distances, symbolized s, are supposedly measured in units such that the cc over a unit distance is 0.99. Suppose, however, distances are measured in km, and symbolized s'. Then the distance so measured, over which the cc is 0.99, is defined as the scale distance and is symbolized r (km). It is given by

$$r = s'/s \quad . \tag{27}$$

Given two of r, s', or s the third is obtained by this equation. Both s' and r must be measured in the same units (for example, km), and s is dimensionless.

4.1 Model A with Scale Distance (r)

Putting $A = 50$ in (22) the cc of Model A decreases as the square of the distance, thus:

$$\rho(s') = \exp\{-(s'/10r)^2\} \quad . \tag{28}$$

4.2 Model B with Scale Distance (r)

Putting $R_o = 64$ in (25), and using (24):

$$\rho(s') = \frac{2}{\pi}\left[\sin^{-1}\sqrt{1-\sigma^2} - \sigma\sqrt{1-\sigma^2}\right],$$

where

$$\sigma = s'/128r \quad . \tag{29}$$

5. SYNOPTIC MAPS - MODELS A AND B

For a computer exercise, the square grid (Figure 2) was chosen to consist of 97 rows and 97 columns. To produce each map random numbers (y_o) were initially assigned to each of the 97 × 97 grid points. The radius of influence (R_o) of Model B was chosen equal to 16 units. The choices of 97 × 97 grid points and $R_o = 16$ were dictated by computer economics.

Through (15) and (20) for Model A or (23) for Model B, the random number at each point (i, j) on the central 65 rows and 65 columns was replaced by y(i, j). The summations required in (15) were extended only to those 797 points within the 16-unit radius circle surrounding the point (i, j). For a radius of influence $R_o = 16$, the cc in Model B between points that are one unit distance apart is $\rho = 0.96$. To obtain the same cc one unit distance apart in Model A the parameter was made A = 12.50.

One sample set of initial random numbers, processed first by Model A, then by Model B, produced the results as shown (Figure 4). In a 9-row by 9-column area, the Model A values of y(i, j) varied from a high of 2.4 to a low of -1.3. In Model B there was a smaller range of y(i, j) in the same area, because the spatial cc maintains a much higher value throughout the area. But whereas in Model A smooth isopleths can usually be drawn around well-formed centers of low and high, in Model B the field is frequently erratic. As a digression from the main theme of this paper, an inference can be drawn from this result with regard to the spacing of weather stations. If the process in nature resembles the Model A process then

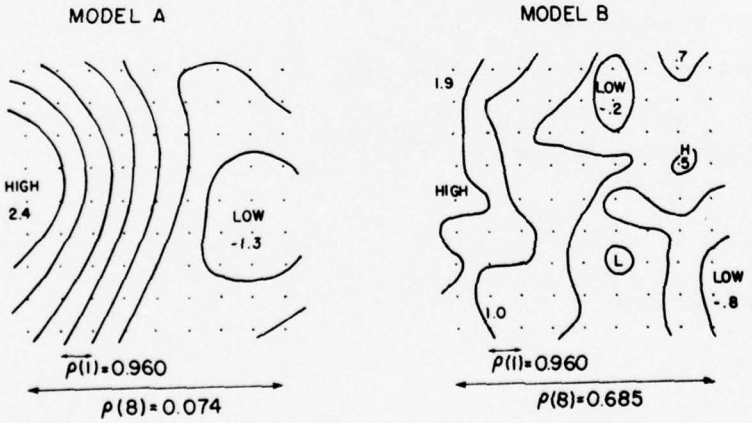

Figure 4. Sample Synoptic Fields Produced By Model A and Model B from Some Initial Set of Random Numbers Assigned to the Grid Points

relatively few observation points will be needed to complete the drawing of isopleths with reasonable accuracy. If, however, the natural process resembles Model B, then even with closely spaced observations some significant events might be missed by the network of stations.

In the example shown in Figure 5 an initial set of random numbers produced a similar typical result. Supposing that the frequency of a cloud cover corresponds to $y < -0.5$, and the frequency of rainfall corresponds to $y < -1.0$, then the Model A picture shows a large single cloud cover with well-defined boundaries and a single large patch of rain. The Model B picture shows more irregularity in the boundary of the cloud cover and separate small patches of cloud and breaks in the main cloud deck; also rainfall is represented by two cells within the large cloud. If the dimension of Figure 5 is of the order of 67 km, then Model B appears to be a better simulator of the mesoscale characteristics of clouds and rainfall, especially summertime rainfall.

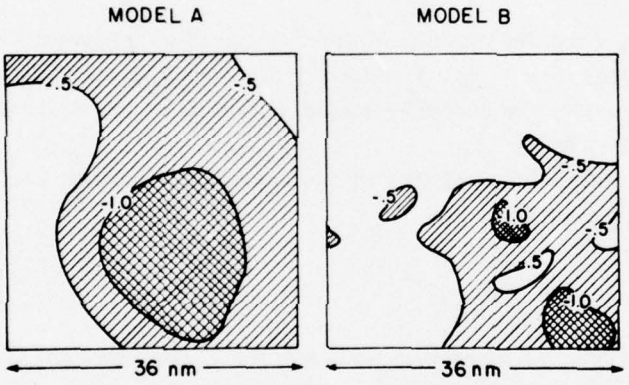

Figure 5. Comparison of Two Pictures of Supposedly Cloud Cover (single hatching) and Precipitation (double hatching). The images are stochastically produced by Model A and Model B from the same initial set of random numbers

6. PROBABILITY DISTRIBUTION OF SPATIAL MINIMUM (OR MAXIMUM)

For a selected model with given function F(R) the simulation program produces a horizontal map (for example, Figures 4 or 5). Repeated M times, it will produce M different maps. At any one point (i, j) of the grid (Figure 2) the M values of y(i, j) from the M maps will collectively have a Gaussian distribution, for M large.

Suppose (s + 1) simultaneous consecutive values of y(i, j) along a single row (j = constant) are examined for a minimum. From M maps there will be M values of the (s + 1) - station minimum, thus giving a frequency distribution of the minimum along a line of travel of length s units. Such simulation is used as this paper's estimate of

$$P(y_{min};s) \quad ,$$

defined as the probability that the minimum of y along a straight-line segment of length s units will be equal to or less than y_{min}.

Suppose that the $(s + 1)^2$ simultaneous values of a part of the grid, that forms a square with sides s units long, are examined for a minimum. From M maps there will be M values of the $(s + 1)^2$ - station minimum, thus giving a frequency distribution of the minimum in an area of s^2. Such simulation is used as this paper's estimate of

$$P(y_{min};s^2) \quad ,$$

defined as the probability that the minimum value of y throughout the area s^2 will be equal to or less than y_{min}. The density of stations is assumed great enough to permit us to consider the $(s + 1)^2$ - station minimum as the minimum of continuous values inside the area.

A reversal of the signs of all y in this exercise, yields the corresponding results for the maximum

$$P(y_{max};s) \quad ,$$

defined as the probability that the maximum of y along a straight-line segment of length s will be equal to or less than y_{max}, and

$$P(y_{max};s^2)$$

defined as the probability that the maximum of y throughout the area s^2 will be equal to or less than y_{max}.

It is clear that a practical exercise, as described above, can produce only approximations by simulation to the probabilities of spatial minima or maxima. The approximations will be improved with a very fine mesh (Figure 2) or with very many rows and columns and strong persistence between adjacent points. However, limitations of computer time made it necessary to use relatively few rows and columns for manageable sample sizes, as described below. For larger areas the

sample size (M) was made smaller, and the persistence between adjacent points was reduced by making the parameter smaller.

6.1 Model A Distribution

With the parameter in (20) set at A = 50, then (22) gives the cc over a unit distance (s = 1) as $\rho = 0.99$. The weighting function F(R), beginning with 1.0 at (i, j), drops as low as 0.006 at a radial distance of 16 units from point (i, j). For $17 \leq i, j \leq 25$ the maps were square, 8 units to the side. Taking M = 10,000, the sample size was large enough to give values of $P(y_{min};s)$ and $P(y_{min};s^2)$ that, when plotted on probability paper, permitted the reasonably accurate drawing of the parts of the curves of y_{min} in Figures 6 and 7 for $s \leq 8$. The curves in Figures 6 and 7 are drawn for $y_{min} = -3.5\ (0.5)\ 3.0$. The s-scale on the horizontal axis is logarithmic and begins on the left side at s = 1/2. There is also a uniform z-scale on the horizontal axis, where

$$z = \ell n s / \ell n 2 \quad . \tag{30}$$

On the ordinate, y_{min} is considered to be simply y(0, 1), that is, the minimum in an infinitesimal area or on an infinitesimally small line segment. The cc is 0.99 over the distance s = 1.

To extend the results to larger areas, up to s = 128 or z = 7, the parameter in (20) was set at A'' = 12.5, and the maps were made squares of 64 units to the side ($17 \leq i, j \leq 81$). With distances symbolized as s'', the cc for s'' = 1 in (22) is 0.9608. This is the same cc at distance s = 2 when A = 50. In general s = 2s''. For the part of the curve where $8 < s \leq 128$, the sample size was made M = 1000, and the results were plotted and drawn continuous with the previous segments for s between 1/2 and 8 units.

To extend the results to a still longer distance and larger area, up to s = 256 or z = 8, the parameter was made A'' = 3.125 for which s = 4s''. Again the sample size was made M = 1000, and the results were plotted and smoothed with the previous results.

In Figures 6 and 7 the y(0, 1)-scale is the scale of y_{min}, and the values for $P(y_{min};s)$ or $P(y_{min};s^2)$ are read on the left-hand scale. If the signs of y(0, 1) are reversed then the values of $P(y_{max};s)$ or $P(y_{max};s^2)$ are read on the right-hand vertical scale.

6.2 Model B Spatial Minimum (or Maximum)

In this model it would not be feasible to have a radius of influence $R_o = 64$, since it would require close to 13,000 random numbers initially to obtain a value of

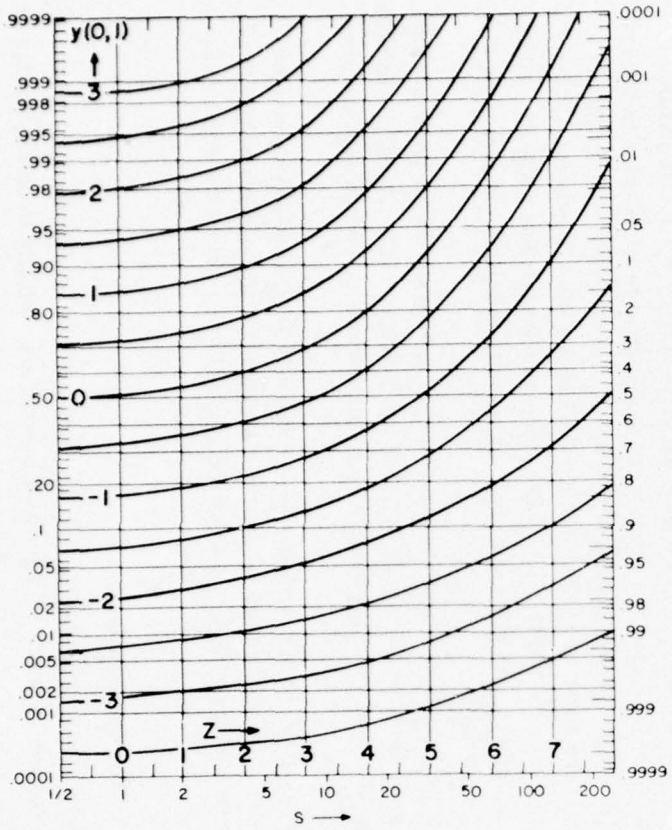

Figure 6. Model A Probability Estimates of the Minimum Value of y(0, 1) Along a Line Segment of Length s Units. The vertical scales are cumulative probabilities. Of the two horizontal scales, one is logarithmic for distance s. The other is the uniform scale of $z = \ell n\, s / \ell n\, 2$. The curves are for values of $y_{min} = -3.5\ (0.5)\ 3.0$

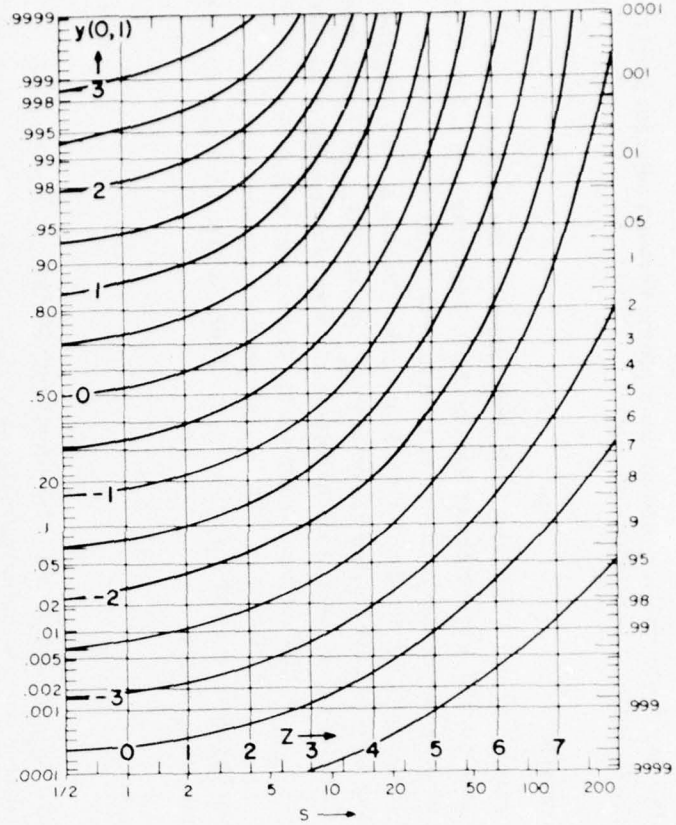

Figure 7. Model A Probability Estimates of the Minimum of y(0, 1) in an Area of Size s^2. Details of the chart are similar to those in Figure 6

y at each point (i, j). With the radius of influence set at $R_o'' = 16$, then (24) gives the cc over a unit distance ($s'' = 1$) equal to 0.9602. This is the same cc as at distance $s = 4$ when $R_o = 64$. For $s = 1$, the cc remains 0.99. In general $s = 4s''$. The weighting function is 1.0 throughout the circular area of radius R_o''. For $17 \leq i, j \leq 25$ the maps were square, 8 units to the side. Taking $M = 75,000$, the values of $P(y_{min};s)$ and $P(y_{min};s^2)$ were estimated to a high degree of accuracy, which permitted drawing the curves for $s \leq 32$ (Figures 8 and 9).

To extend the results to larger areas, up to $s = 256$ or $z = 8$, the sample size had to be reduced ($M = 5000$) to obtain estimates within a reasonable time of computer operation. The synoptic maps were squares, 64 units to the side for $17 \leq i, j \leq 81$. The results for the minima were plotted and smoothed with the previous results.

The scales in Figures 8 and 9 have similar descriptions as those in Figures 6 and 7 and the charts are used in similar fashion.

6.3 Model B Highest Minimum (or Lowest Maximum) in a Fractional Coverage of an Area

Each model, as described so far, provides an estimate of the probability of a minimum or maximum condition in a region of stated size. But there is still a requirement to estimate the probability that a certain percentage or fraction of a given area will experience a critical event or a threshold condition. For example, in the case of heavy 24-hr rainfall (≥50 mm), it might be desirable to know the probability that one-fourth or one-half of a city will receive this amount, compared with the lesser probability that the whole city of, say, 100 km^2 will be drenched.

In a horizontal map (for example, Figure 4) suppose that the $(s + 1)^2$ simultaneous values (y) are sorted from the largest to the smallest (y'). Then the first $f(s + 1)^2$ values of y' will be equal to or greater than their last value. Any other selection of a fraction (f) from the $(s + 1)^2$ values of y will have a lower minimum. From M maps there will be M values of $y'\{f(s + 1)^2\}$, to provide a frequency distribution of the maximized minimum in the fractional coverage (f) of an area (s^2). Such simulation is used as this paper's estimate of

$$P(y_{maxmin};s^2, f) \quad ,$$

defined as the probability that, in a fraction f of the area s^2, the highest possible minimum value of y is y_{maxmin}. A reversal of the signs of all y's in this exercise yields the corresponding results for the minimized maximum

$$P(y_{minmax};s^2, f) \quad ,$$

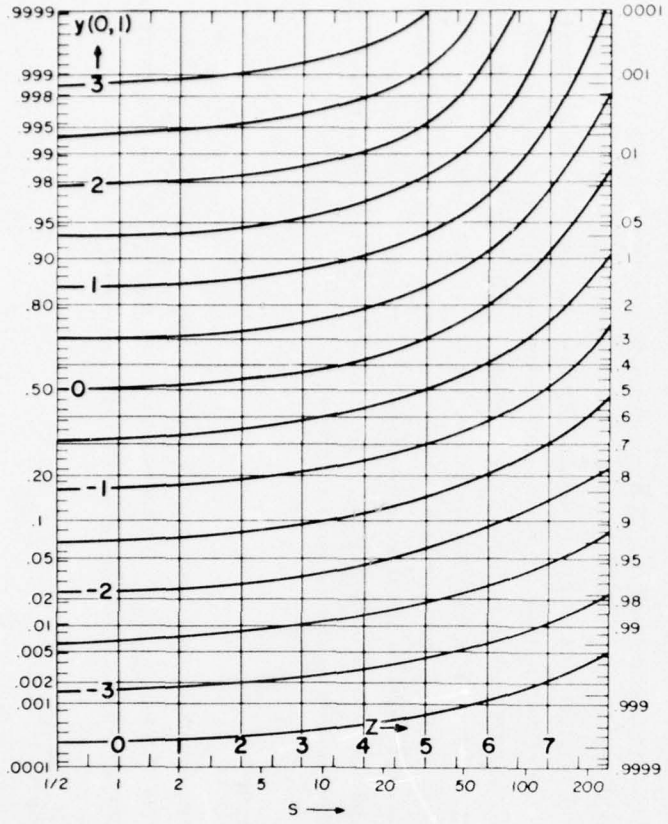

Figure 8. Model B Probability Estimates of the Minimum of y(0, 1) Along a Line Segment of Length s. Details of the chart are similar to those in Figure 6

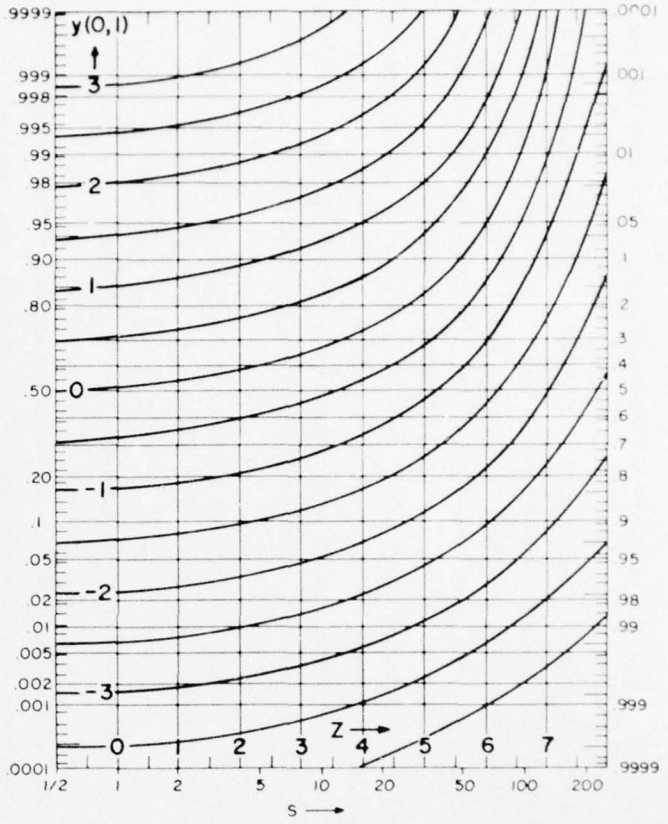

Figure 9. Model B Probability Estimates of the Minimum of y(0, 1) in an Area of Size s^2. Details of the chart are similar to those in Figure 6

defined as the probability that, in a fraction f of the area s^2, the lowest possible maximum value of y is y_{minmax}.

Model B was chosen for further exploration by Monte Carlo procedure, since it proved to be the more effective model on precipitation (see Section 7). In each synoptic map, consider the smallest square in the grid (any square). With four values of y, one at each corner of the smallest square, when ordered by size, the ith value can be considered to be the ith largest (i = 1, 4) in a sample of four values taken from the infinite population in the unit area. Consider the square of 2 units to each side. When the 9 associated values are ordered by size, the ith value is considered to be the ith highest in a sample of 9 taken from the infinite population of the area. In general, in a square of s units to one side, when the $(s + 1)^2$ values are ordered by size, the ith value is the ith highest in a sample of $(s + 1)^2$ values. The fraction (f) of the area represented by the i values[7] is estimated by

$$f = (i - 3/8)/\{(s + 1)^2 + 1/4\} \tag{31}$$

In the Monte Carlo exercise the number of synoptic maps generated from initially random numbers was M = 5000. Each map was 64 units to one side, so that seven square areas, of sizes 1^2, 2^2, 4^2, 8^2, 16^2, 32^2, 64^2 could be studied. But the field was produced for a radius of influence $R_o' = 16$, so that the cc between stations one unit apart (s' = 1) was 0.9602. That is, the smallest square is actually 4 units to a side (s = 4), when measured by that element of length over which the cc is 0.99.

Consider an elementary area of one square (s' = 1 or s = 4) with the four corner values of y ordered by size. For M = 5000 the cumulative distribution of values of y_{maxmin} for the first, second, third, and fourth values were plotted (Figure 10) at fraction (f) of the area given by (31). On the left-hand ordinate (Figure 10) the probability is that of the highest minimum in an infinitesimal fraction of the area, in other words the areal maximum, as obtained from Figure 9 (at s = 4 or z = 2). On the right-hand side the cumulative probability is that of the minimum of the whole area, again obtained from Figure 9 (at s = 4 or z = 2). Thus, each y-curve, y = -3.5 (0.5) 3.5, was drawn through six points, at each end and at f = 0.147, 0.382, 0.618 and 0.853.

Consider the larger area (s' = 2 or s = 8) of 4 squares composed of 9 grid values of y that are then ordered by size. In the large sample, M = 5000, the distributions of each of the 9 values of y' were plotted, in accordance with (31) at f = 0.0757, 0.197, ···, and 0.932, along with the distribution of the minimum

7. Blom, Gunnar (1958) Statistical Estimates and Transformed Beta-Variables, John Wiley and Sons New York.

on the right-hand side and the maximum on the left-hand side, as found in Figure 9 at s = 8 (or z = 3). The chart so produced was similar to Figure 10. Likewise, similar charts were drawn for the areas 4^2, 8^2, 16^2, 32^2, and 64^2. The isopleths of all seven such charts provided points for the plotting of Figures 11 to 19 for the highest 1/10, 2/10, ···, highest 9/10. The last chart of this series, for the highest 10/10, would be identical with Figure 9.

Figures 11 to 19, together with Figure 9, comprise the substance of this section and provide the means for determining the probabilities of fractional cover of a given area by a describable event. At first glance the charts seem to present a few surprises, but upon further reflection the results are reasonable. For example, an event that has a 50 percent chance of occurring at one single point will occur with greater probability (read right-hand scale) over 1/10 to 4/10 of the area. On the other hand, this probability must decrease for fractions of the area greater than one-half. Again, for a rare event of, say, 1 percent single-point probability, the chances are improved, to as much as 3 percent of its occurring in 1/10 of the area – up to a certain optimum areal size. But as the area is further enlarged, the probability of the rare event covering as much as 1/10 of the increasingly larger area begins to vanish.

7. APPLICATIONS

For the most direct application of either Model A or Model B to a weather element (X) the input consists of the single-point frequency distribution, P(x), plus one additional parameter: the scale distance (r). Through the graphs (Figures 6 through 9, 11 through 19) the information is used to estimate the probability of occurrence along a line of given length, or within an area of given size or a fraction of the area.

For a one-to-one correspondence between x and y, as defined in (1), let us further define:

$P_o = P(x_{min}) = P(y_{min})$, the probability that x will not exceed x_{min} at a single selected point.

$P_s = P(x_{min};s') = P(y_{min};s)$, the probability that the minimum of x along a line of length s' (km) will not exceed x_{min}.

$P_a = P(x_{min};s'^2) = P(y_{min};s^2)$, the probability that the minimum of x throughout the area s'^2 (km^2) will not exceed x_{min}.

$P_f = P(x_{maxmin};s'^2, f) = P(y_{maxmin};s^2, f)$, the probability that the maximized minimum of x in a fraction f of the area s'^2 (km^2) will not exceed x_{maxmin}.

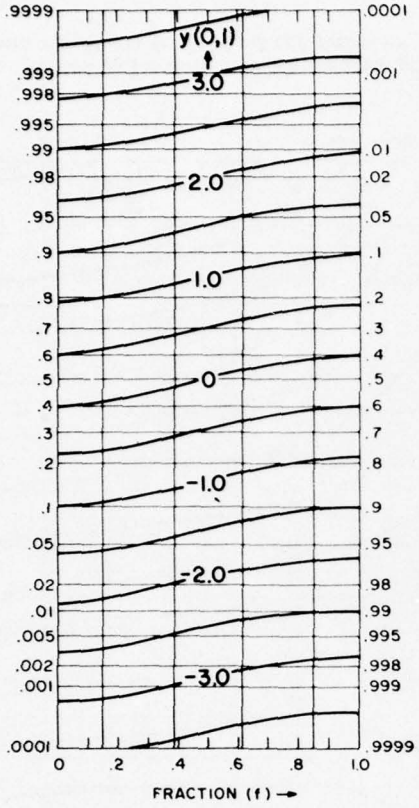

Figure 10. Model B Cumulative Probability of the Highest Minimum of y(0, 1) in a Fraction (f) of an Area of 4^2 Squares (s = 4). The cc between points one unit distance apart is 0.99

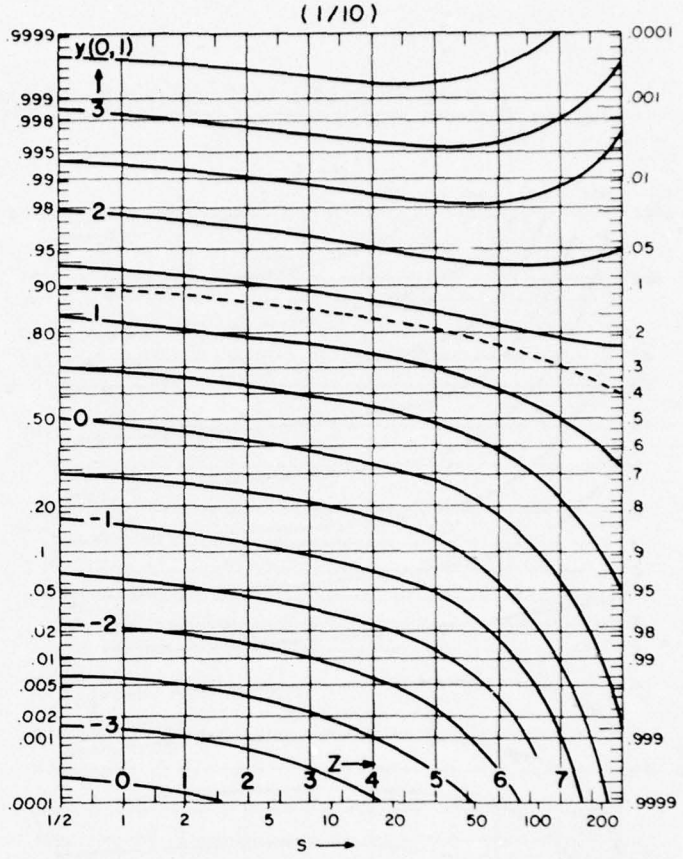

Figure 11. Model B Probability Estimates of the Highest Minimum of y(0, 1) in 1/10 of the Area s^2. Details of the chart are similar to those in Figure 6

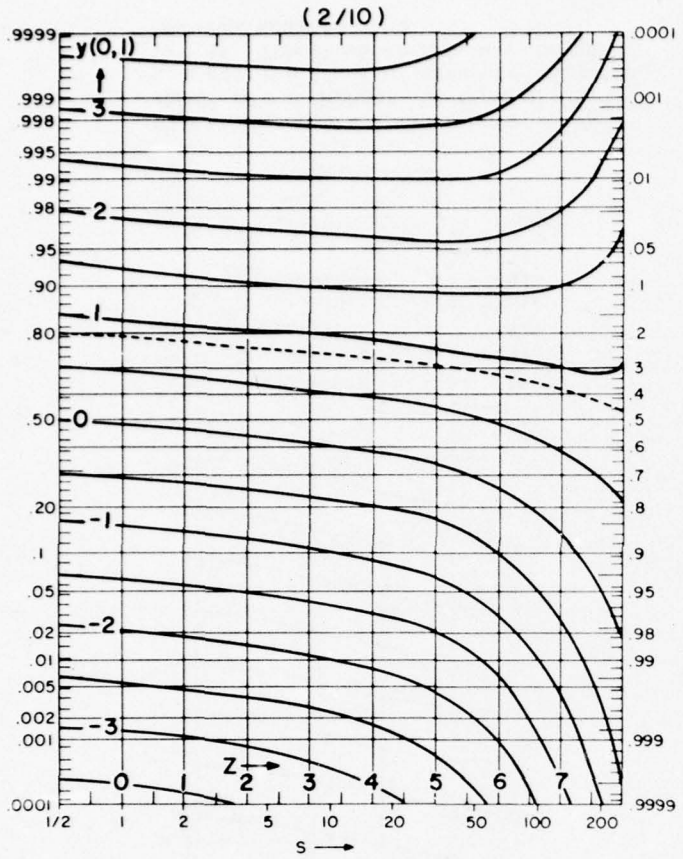

Figure 12. Model B Probability Estimates of the Highest Minimum of y(0, 1) in 2/10 of the Area s^2

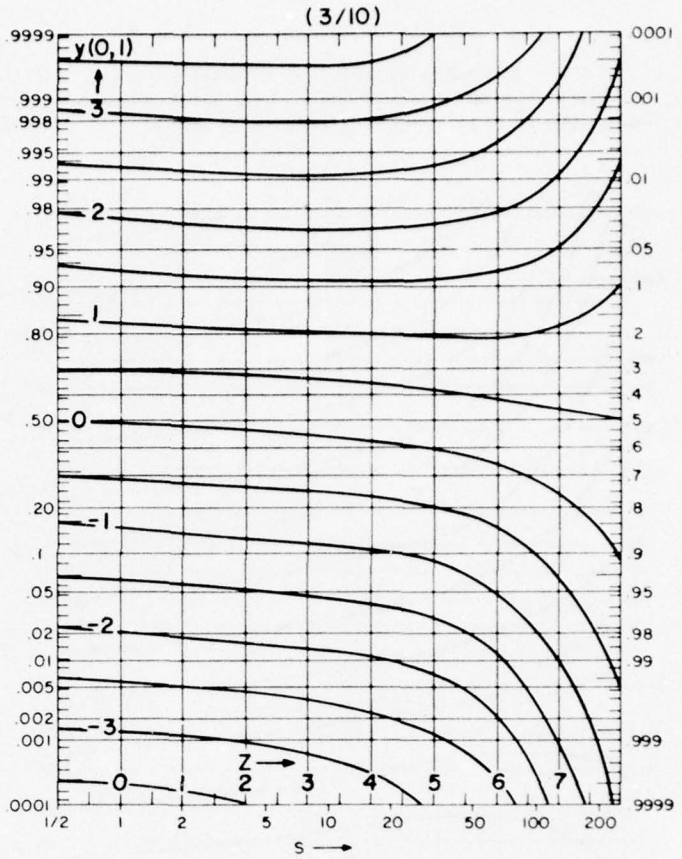

Figure 13. Model B Probability Estimates of the Highest Minimum of y(0, 1) in 3/10 of the Area s^2

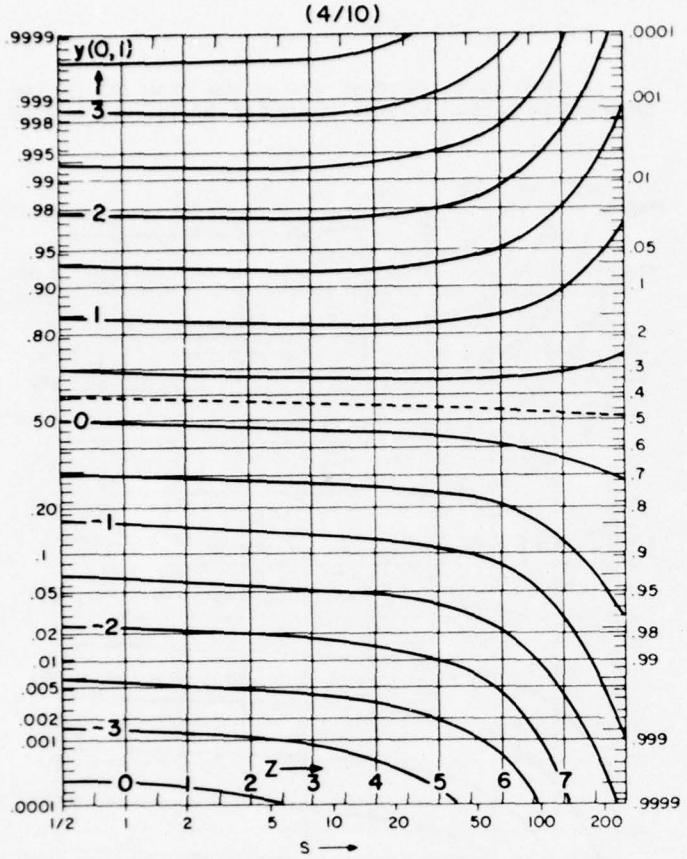

Figure 14. Model B Probability Estimates of the Highest Minimum of y(0, 1) in 4/10 of the Area s^2

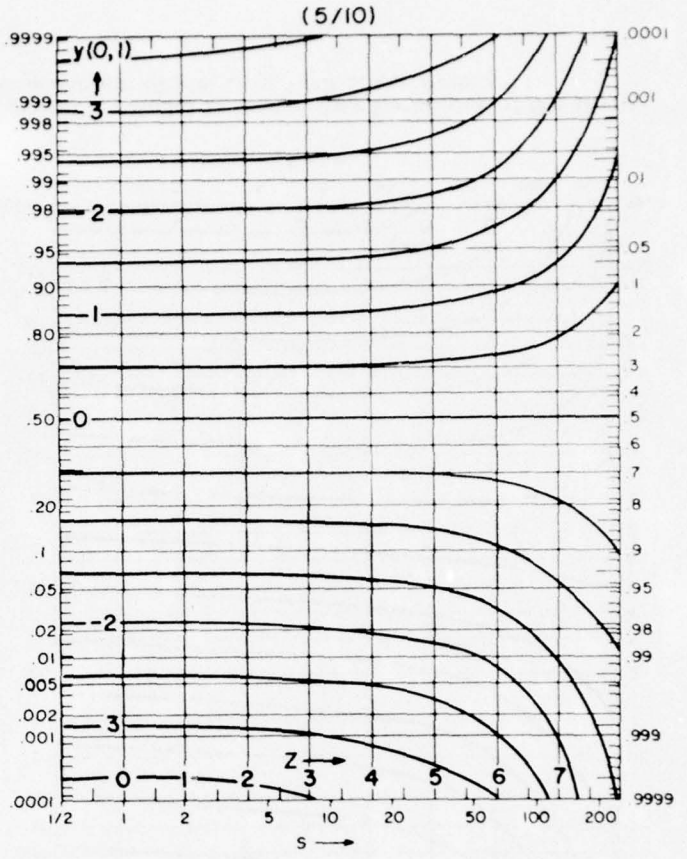

Figure 15. Model B Probability Estimates of the Highest Minimum of y(0, 1) in 5/10 of the Area s^2

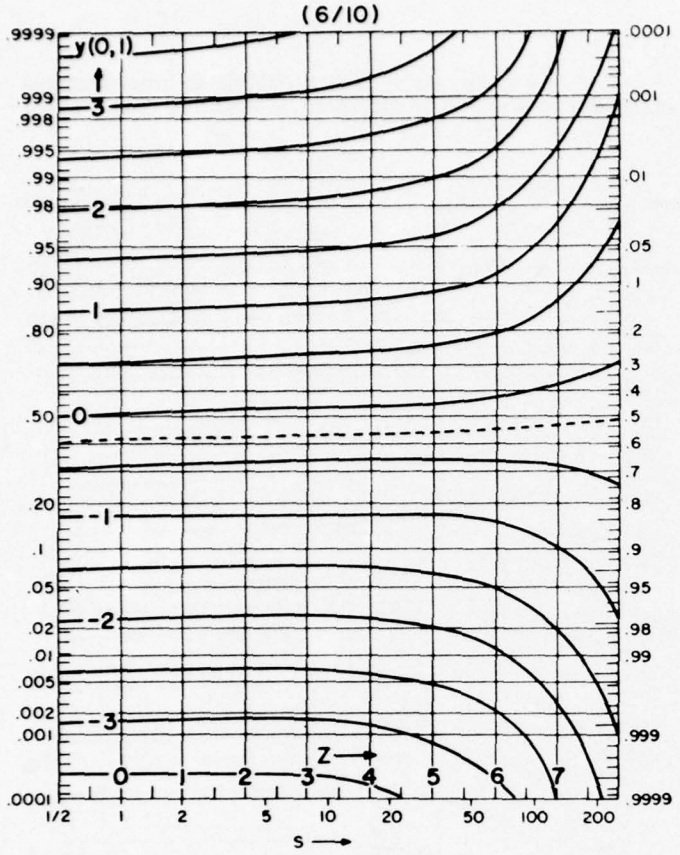

Figure 16. Model B Probability Estimates of the Highest Minimum of y(0, 1) in 6/10 of the Area of s^2

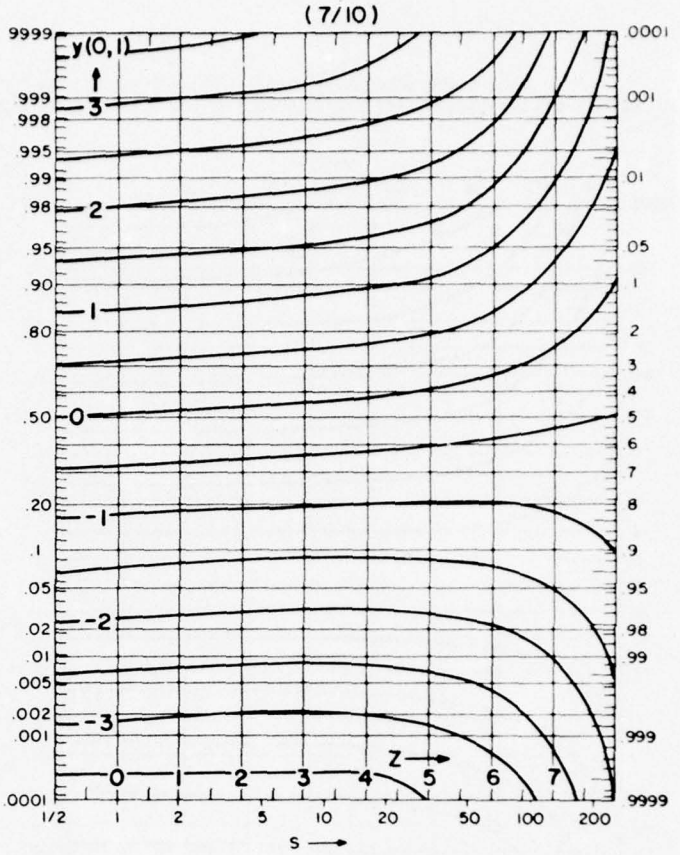

Figure 17. Model B Probability Estimates of the Highest Minimum of y(0, 1) in 7/10 of the Area s^2

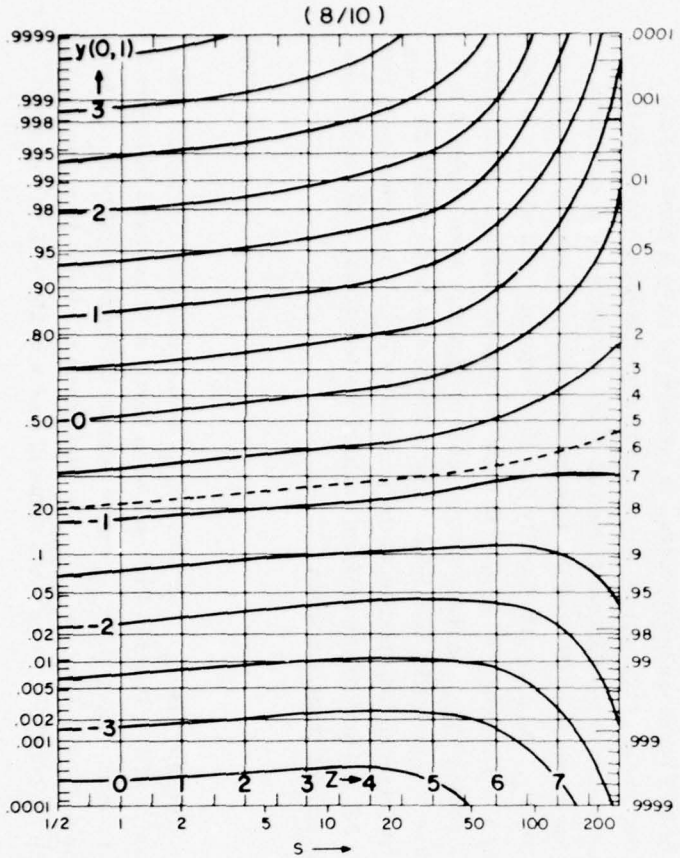

Figure 18. Model B Probability Estimates of the Highest Minimum of y(0, 1) in 8/10 of the Area s^2

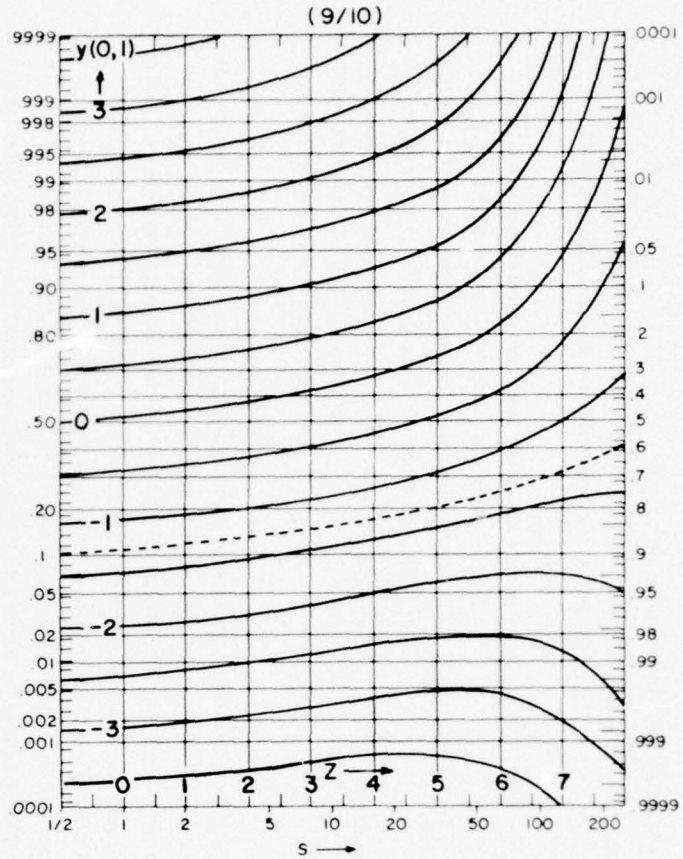

Figure 19. Model B Probability Estimates of the Highest Minimum of y(0, 1) in 9/10 of the Area s^2

When the subject is spatial maximum we define:

$P_o = P(x_{max}) = P(y_{max})$, the probability that x will not exceed x_{max} at a single point, essentially the same definition when $P_o = P(x_{min})$.

$P_s = P(x_{max};s') = P(y_{max};s)$, the probability that the maximum of x along a line of length s' (km) will not exceed x_{max}.

$P_a = P(x_{max};s'^2) = P(y_{max};s^2)$, the probability that the maximum of x throughout the area s'^2 (km^2) will not exceed x_{max}.

$P_f = P(x_{minmax};s'^2, f) = P(y_{minmax};s^2, f)$, the probability that the minimized maximum of x in a fraction f of the area s'^2 (km^2) will not exceed x_{minmax}.

In the following examples, procedures were followed to produce an estimate of scale distance (r), which then becomes a telling characteristic of the weather element under investigation. In Model A or Model B the larger the value of r the greater is the horizontal persistence of the element. The first example, below, is of the macroscale 100-mb wintertime temperature field in the northern hemisphere. The second example is of the horizontal extent of New England rainfall. With respect to rainfall a difficulty arises because of its integration over a time interval, like one hour or one full day. The third example, on the other hand, consisting of a study of PPI radar-scope pictures, is considered to be a more logical application of the model of this paper, since each picture is closer to an instantaneous representation of the horizontal spread of the meteorological condition.

Suppose, for an element (X) that the climatic frequency is used as an estimate of the probability P_o. Suppose additionally that the frequency with which x is the minimum along a line of length s' is used to estimate probability P_s. Each value of P_o defines a value of y_{min} on the ordinate scale of Figure 6 when Model A is used, and Figure 8 when Model B is used. The value of s is found where the y_{min} curve (generally interpolated) intersects the probability P_s. More practically the value of z (Eq. 30) is found on the uniform scale of the horizontal axis, and then s is obtained through the transformation

$$s = 2^z \quad . \tag{32}$$

Likewise if the frequency is P_a, with which x_{min} is the minimum throughout the area s'^2, the value of s is found in Figure 7 when Model A is used and in Figure 9 when Model B is used, where the y_{min} curve intersects the probability P_a. Again, if the frequency is P_f, with which x_{maxmin} is the highest minimum in a fraction f of the area s'^2 for f = 1/10, ···, 9/10, the value of s or z in Model B is found in

Figure 11, Figure 12, ···, or Figure 19, respectively, where the y_{maxmin} curve intersects the probability P_f. Each ratio of s' to s is an estimate of the scale distance (r).

For m(a) values of X in the ath areal size, and for n areal sizes, there will be N estimates of the scale distance (r) where

$$N = \sum_{a=1}^{n} m(a) \quad . \tag{33}$$

The proximity, to each other, of all individual estimates of r is a measure of the effectiveness of the model. The order of magnitude of the values, as in the examples below, could appear to reveal a damaging lack of similarity in the judgment of the reader. But the models were useful in application and a single "best" estimate was well justified.

How should the "best" single estimate of r be obtained? Since r is the ratio of s' to s, the errors on the low side are bounded by zero, but on the high side the errors are unbounded. On the other hand, $\ell n\ r$ is equally unbounded on both the low and the high side. Moreover, since the graphs (Figures 5 through 9, 11 through 19) are constructed with a uniform scale of z, which is proportional to $\ell n\ s$, the errors in estimating $\ell n\ s$ tend to be more equally divided above and below a true value than they would be in estimating s. Consequently, it is preferable to take the average of $\ell n\ r\ (=\ell n\ s' - \ell n\ s)$ than the average of r per se. This is the same as taking the geometric mean of r, as follows:

$$\hat{r} = \left[\prod_{i=1,\, a=1}^{m(a),\, n} (s_a'/s_{ai}) \right]^{1/N} \quad . \tag{34}$$

In practice each value of z is obtained from the appropriate curve (Figures 6 through 9, 11 through 19) by using each pair of P_o and P_s, or P_a, or P_f. For the ath area the average value of z is given by

$$\bar{z} = \sum_{i=1}^{m(a)} z_i/m(a) \quad , \tag{35}$$

which yields

$$\hat{s}(a) = 2^{\bar{z}} \quad , \tag{36}$$

which, when divided into s'(a), yields

$$r(a) = s'(a)/\hat{s}(a) \quad . \tag{37}$$

Then, lastly, a single estimate of r is obtained by

$$\hat{r} = \left[\prod_{a=1}^{n} \{r(a)\}^{m(a)} \right]^{1/N} \quad . \tag{38}$$

7.1 Example 1: 100-mb Route Temperatures

Climatological maps of the northern hemisphere temperature at supersonic transport altitudes have been published by season in percentiles from 2 to 98.[8] Each map is accompanied by a graph that provides an estimate of the probability that the temperatures on a given route and midlatitude will remain above the temperatures that are on the map along that route. For the 100-mb level, wintertime, these probabilities (P_s) are as shown in Table 2 for routes of varying length from 1000 km to 9000 km, with midlatitude 45°N. The probability estimates (P_s) had been made by actual sampling of the data on synoptic charts.

Model A (Figure 6), when applied to the values of P_o and P_s (Table 2), yields values for z, one value corresponding to each pair of P_o and P_s. Consequently, through (32), (27), (37), Model A yields an estimate of scale distance, $\hat{r}$ = 289 km, which, when applied in (28), gives a decrease of cc with distance as shown (Figure 20). Also shown is Bertoni and Lund's[9] curve for the decrease of temperature cc between pairs of stations at the 16-km level (near 100-mb). In contrast with Bertoni and Lund's data this author's data were taken from smoothed synoptic analyses of 100-mb surfaces, which would tend to increase the apparent horizontal relationship between stations. Moreover, the Bertoni and Lund temperatures were derived from radiosonde data. Hence the temperatures on constant-level surfaces (rather than constant-pressure) might have additional errors, causing faster cc decay and calling for a smaller scale distance (see below).

Model B (Figure 8) yielded the other estimates for z as shown in Table 2 and a consequent scale distance $\hat{r}$ = 85.6 km. When used in (29) and (24) the decay of cc becomes as shown (Figure 20). Clearly Model A is preferable for the macroscale upper-air temperatures.

8. Gringorten, I.I. and Tattelman, P. (1970) Point and Route Temperatures for Supersonic Aircraft, AFSG, No. 233, AFCRL-70-0420, Bedford, MA.

9. Bertoni, E.A. and Lund, I.A. (1964) Winter Space Correlations of Pressure, Temperature and Density to 16 km, ERP, No. 75, AFCRL-64-1020, Bedford, MA.

Table 2. The Cumulative Probability (P_s) of the Minimum Temperatures (percentile P_o) at 100 mb, Wintertime, Along a Route Whose Midlatitude is 45°N. The probability that the temperatures enroute will equal or exceed the percentile (P_o) is (1 - P_s). For the last three columns see text

Percentile P_o	Temps on map (°C) Equator to N-pole	Route length (km) s'	P_s	Z		When r=185 km $\hat{P}_s$
				Model A	Model B	
0.02	-88	1481	0.03	1.62	3.16	0.045
	to	2130	0.04	2.61	4.26	0.055
	-55	3148	0.05	3.21	4.90	0.069
		4908	0.07	4.17	5.78	0.089
		7223	0.10	4.97	6.65	0.109
		8519	0.11	5.18	6.81	0.128
0.10	-82	1074	0.12	1.82	2.25	0.170
	to	1824	0.15	2.05	3.71	0.205
	-53	3148	0.20	3.22	5.00	0.268
		4815	0.25	3.91	5.83	0.336
		6112	0.30	4.44	6.33	0.380
		7130	0.35	4.80	6.74	0.412
		8704	0.40	5.16	7.06	0.470
0.25	-81	1130	0.30	1.10	2.5	0.375
	to	1611	0.35	2.22	3.70	0.420
	-50	2797	0.40	2.93	4.58	0.50
		3704	0.50	3.90	5.73	0.565
		4630	0.55	4.21	6.09	0.620
		6112	0.60	4.53	6.44	0.695
		7408	0.70	5.08	7.10	0.745
		9075	0.80	5.63	7.65	0.800
0.50	-80	1296	0.60	2.00	3.51	0.66
	to	1778	0.65	2.68	4.37	0.707
	-48	2426	0.70	3.17	5.05	0.76
		3704	0.80	4.01	6.00	0.84
		6297	0.90	4.82	6.85	0.927
		8704	0.95	5.36	7.36	0.964
0.75	-79	982	0.80	1.26	2.80	0.85
	to	1463	0.85	2.40	4.30	0.884
	-45	2593	0.90	3.24	5.26	0.934
		4630	0.95	4.08	6.18	0.975
		7778	0.99	5.14	7.15	0.9945
0.90	-78	1306	0.95	2.28	3.88	0.965
	to	3148	0.98	3.47	5.38	0.9917
	-43	4352	0.99	4.00	5.93	0.9967
0.98	-77 to -41	1389	0.99	1.76	3.35	0.9953

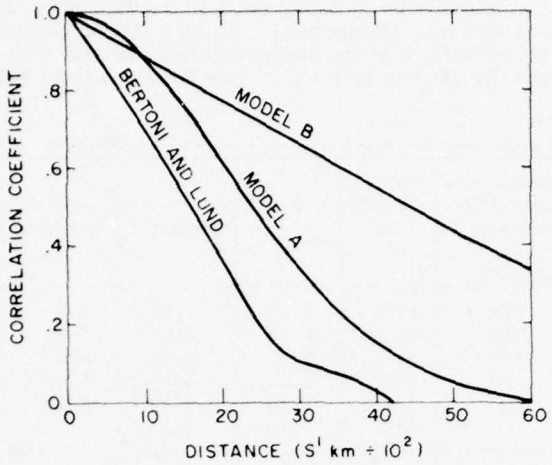

Figure 20. Decrease of 16-km Temperature cc with Distance Between Stations, as Found by Bertoni and Lund (1964), and the Model A and Model B Estimates of the Decrease on the 100-mb Surface

An application of Figure 6 or Figure 7 together with an assigned value of the scale distance (r) provides a method for obtaining the probability of the minimum percentile of route temperature, or the minimum in an area of given size. It is still necessary to have geographic charts showing what temperatures correspond to the percentiles of 0.02, $\cdots$, 0.99.

Suppose the problem is to find P_s versus s', knowing the cc decrease with distance as given by Bertoni and Lund (Figure 20). For Model A the Bertoni and Lund curve yields a geometric mean value of the scale distance, $\hat{r}$ = 185 km, which is 36 percent shorter than the estimate using the 100-mb data. Hence, with less horizontal persistence, it is to be expected that low minima will be predicted with greater probability. Using r = 185 km to obtain values of z from (27) and (30) to correspond to the values of s' in Table 2, and entering z in Figure 6, estimates ($\hat{P}_s$) were obtained as shown in the last column of Table 2. On the average, these latter probability estimates are 13 percent higher.

7.2 Example 2: Rainfall Frequencies

Recent monthly publications of the National Weather Service reveal that there are more than 350 stations at which 24-hr rainfall is observed, once per day, throughout New England. Such a network does provide a good areal coverage of precipitation. But it confronts this study with several difficulties. First of all the

cooperative observers do not have a single time at which to read the 24-hr cumulation of precipitation. At most stations the rain gauge is read at 0800 Local Time. But many observers read the amount in the afternoon, some at midnight. Hence, a survey of rainfall amounts, to obtain the 24-hr maximum, would be faulty unless the data were used only from stations taking observations at the same time.

Some 100 stations report precipitation amounts hourly and they provide 24-hr amounts ending at midnight. With the study limited to these stations, the maximum daily precipitation was recorded in each of the areas shown in Table 3.

Table 3. Showing Areas of Increasing Size, Beginning with Massachusetts and Ending with All of New England. The distance s'(a) is the square root of the ath area

States	Area no. (a)	Area km^2	s'(a) km
MA	1	21358	146.1
MA,RI,CT	2	37455	193.5
MA,RI,CT,NH,VT	3	86377	293.9
MA,RI,CT,NH,VT,ME	4	172294	415.1

(1) New England January 24-hr Precipitation

The precipitation data presented in the National Environmental Data Service monthly bulletins (U. S. Dept. of Commerce, 1952-1972) were surveyed to obtain the climatic frequency (P_o) of 24-hr precipitation and the frequency of maximum (P_a, for a = 1, 2, 3, 4) in the successively larger areas of New England beginning with the 21,358 km^2 of Massachusetts (Table 4). The true climatic frequencies of precipitation are assumed to be the same for all four areas and therefore the differences in P_o shown in Table 4 are assumed to be sampling errors from true probabilities. For the intended purpose of finding the parameter (r), each frequency (P_o) is used in conjunction with the frequency of the maximum precipitation (P_a) for its area. Table 4 presents only a fraction of the cumulative frequencies used for 24-hr rainfall. Actually used were the cumulative frequencies as follows: none or trace, 0.25(0.25)2.3, 3.6, 4.8, 7.4(2.54)27.7, 37.8(12.70)88.6 mm.

Each value of P_o was entered on the left-hand ordinate of Figure 9, although read on the right-hand scale. The P_o curve, usually interpolated, was followed until the value of P_a was reached, then the value of z on the abscissa was read

Table 4. A Partial Summary of the Cumulative Relative Frequency and the Resulting Value of z (see text) of New England January 24-hr Precipitation in 21 Years (1952-1972). The frequencies (P_o) were based on the records of those stations and years when the 31-day records were complete. The symbols used are as defined in the text. Areas 1 to 4 are defined in Table 3

Amt (mm)	Area 1			Area 2			Area 3			Area 4		
	P_o	P_a	z	P_o	P_a	z	P_o	P_a	z	P_o	P_a	z
none or T	.641	.389	4.06	.656	.362	4.45	.639	.161	5.54	.639	.128	5.81
2.3	.781	.583	3.84	.790	.564	4.23	.786	.400	5.19	.787	.359	5.40
4.8	.845	.720	3.49	.851	.704	3.59	.851	.586	4.80	.853	.545	5.00
9.9	.9139	.802	3.95	.9163	.786	4.23	.9199	.724	4.88	.9211	.692	5.19
15.0	.9476	.856	3.74	.9510	.844	4.23	.9535	.801	4.80	.9541	.776	5.00
20.1	.9690	.9008	4.10	.9707	.888	4.51	.9724	.855	5.10	.9727	.836	5.37
25.1	.9821	.9253	4.19	.9831	.9192	4.57	.9842	.9023	4.99	.9844	.890	5.10
50.5	.9992	.9914	5.10	.9986	.9883	5.05	.9988	.9928	5.29	.9989	.9791	5.79
s'(a)	146.1 km			193.5 km			293.9 km			415.1 km		
m(a)	23			23			23			23		
$\bar{z}$	3.94			4.27			5.14			5.38		
$\hat{s}$(a)	15.31			19.23			35.20			41.71		
$\hat{r}$(a)	9.54 km			10.06 km			8.35 km			9.95 km		

and recorded (Table 4). For the greater extremes of precipitation the observed frequencies became erratic. Hence the values of z were obtained only up to the frequency of 50.5 mm making m(a) = 23 for a = 1, 2, 3, or 4. Through (35), (36), (37) the final value of the parameter in Model B for this region, month, and 24-hr precipitation was estimated at $\hat{r}$ = 9.45 km.

As stated above, the value of $\hat{r}$ = 9.45 km is the estimate of the scale distance, over which the cc is 0.99. Since Model B was used, the cc decreases with distance as given by (24) and (29), as shown in Figure 21. When Model A (Figure 7) was used in a parallel exercise, the scale distance $\hat{r}$ was 30.35 km, which when used with (28) produced the cc decay shown by the second curve in Figure 21. With Model A there is a rapid decrease of the cc with distance between stations, after a separation of 100 km. To demonstrate that this is an unacceptable weakness in applying Model A, rather than Model B, the precipitation data were surveyed by pairing the stations shown in Table 5 to obtain cc more directly.

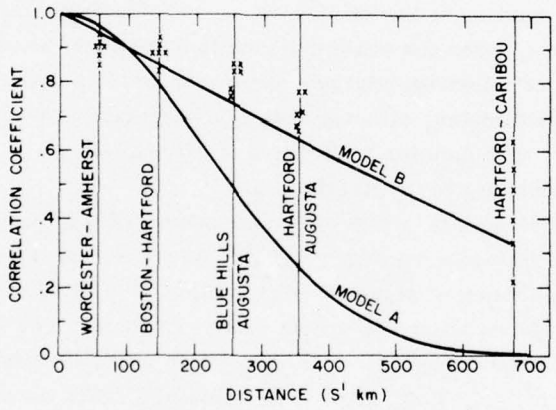

Figure 21. Decrease of cc with Distance (s' km) Between Precipitation at Stations in New England in January. The X's are plotted at six sample estimates of tetrachoric cc between the precipitation of five pairs of stations, based on 1952-1972 data

For each pair of stations there was a joint frequency of 24-hr precipitation equal to or less than: trace, 2.3 mm, 4.8 mm, 7.4 mm, 9.9 mm and 12.4 mm, as well as the unconditional frequency of these amounts at either station. An

Table 5. The Pairs of Stations that Were Selected to Find the cc Between Their 24-hr Precipitation Ending at Midnight. The January cc's are shown plotted in Figure 21, the July cc's are plotted in Figure 22

First Station	Second Station	Distance apart
Worcester, MA	Amherst, MA	56 km
Boston, MA	Hartford, CT	144 km
Blue Hill, MA	Augusta, ME	256 km
Hartford, CT	Augusta, ME	355 km
Hartford, CT	Caribou, ME	678 km

application of the bivariate normal distribution[10, 11] yielded six corresponding estimates of the cc for each pair of stations, as shown plotted in Figure 21. (The cc obtained in this manner is sometimes known as tetrachoric cc.)

Clearly Model A, when the scale distance is determined as above, does not anticipate the high cc's between stations more than 100 km apart. Model B also tends to give underestimates, although they are acceptable for estimating order of magnitude of the cc as a function of distance of separation.

(2) New England July 24-hr Rainfall

The same source of data was used for the survey of the frequency distribution of July rainfall and its areal maximum. Table 6 is a partial list of the results. The frequency distribution of single-station rainfall (P_o), in this case, is an average for some 12 widely scattered stations in New England. The values of z in Table 6 were obtained, through use of Figure 9, up to the frequency of 63.2 mm, making m(a) = 9 for a = 1, 2, 3, or 4. The value of s'(a) is the square root of the ath area. Through application of (35), (36), (37), and (38) the final value of the scale distance for New England July 24-hr rainfall was estimated at r = 5.19 km with Model B.

10. National Bureau of Standards (1959) Table of the Bivariate Normal Distribution Function and Related Functions, NBS Appl. Math. Series, No. 50, Govt. Printing Office, Washington, D.C.

11. Gringorten, I.I. (1971) Modelling conditional probability, J. Appl. Meteorol., 10:646-657.

Table 6. A Partial Summary of the Cumulative Relative Frequencies and the Resulting Values of z (Model B) of New England July 24-hr Precipitation in 21 Years (1952-1972). The symbols are as defined in the text. Areas 1 to 4 are defined in Table 3

Amt (mm)	All Stations (P_o)	Area 1		Area 2		Area 3		Area 4	
		P_a	z	P_a	z	P_a	z	P_a	z
None or T	0.698	0.402	4.40	0.343	4.85	0.182	5.77	0.125	6.09
2.3	0.810	0.525	4.65	0.466	5.03	0.280	5.89	0.214	6.13
4.8	0.858	0.603	4.75	0.540	5.13	0.374	5.85	0.303	6.16
9.9	0.9095	0.712	4.64	0.641	5.12	0.495	5.85	0.431	6.10
15.0	0.9415	0.772	4.90	0.710	5.36	0.586	6.00	0.528	6.21
25.1	0.9720	0.850	5.10	0.796	5.65	0.713	6.13	0.672	6.32
37.8	0.9877	0.9315	4.70	0.896	5.38	0.832	6.05	0.795	6.30
50.5	0.9939	0.9699	4.46	0.9422	5.37	0.9023	6.02	0.865	6.22
63.2	0.9979	0.9868	4.70	0.9683	5.79	0.9499	6.25	0.9407	6.38
s'(a)		146.1 km		193.5 km		293.9 km		415.1 km	
m(a)		9		9		9		9	
$\bar{z}$		4.70		5.30		5.98		6.21	
$\hat{s}$(a)		25.99		39.40		63.12		74.03	
$\hat{r}$(km)		5.63		4.91		4.65		5.61	

When $r = 5.19$ km with Model B the cc decreases with distance as shown (Figure 22). When Model A was used in a parallel exercise the scale distance was estimated at $\hat{r} = 17.63$ km and resulted in the second curve for cc decrease with distance (Figure 22).

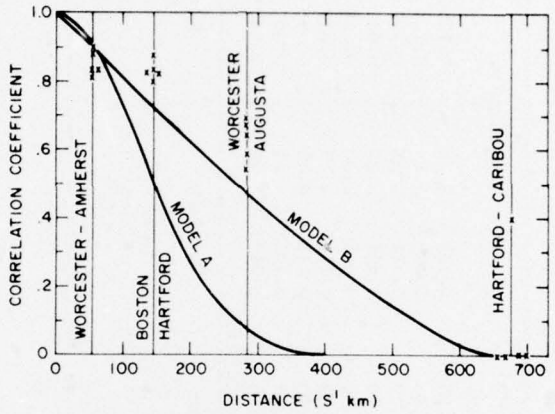

Figure 22. Decrease of cc with Distance (s' km) Between Rainfall at Stations in New England in July. The X's are plotted at five sample estimates of tetrachoric cc between the rainfall at four pairs of stations, based on 1952-1972 data

Shown also in Figure 22 are the cc's, five for each separation of stations, as determined by pairing stations to obtain the joint frequencies of July 24-hr rainfall, dichotomously dividing their distributions at a trace, 2.3 mm, 4.8 mm, 9.9 mm, and 25.1 mm and applying the bivariate normal distribution to obtain tetrachoric cc.

Again Model B tends to underestimate the cc's slightly, while Model A is unacceptable. For the two stations, Hartford and Caribou, separated by 678 km, four of the cc's were estimated at zero (or less).

(3) New Englard January 1-hr Precipitation

Since the above exercises were conducted with 24-hr precipitation, it is possible that the time-averaging effect is to increase the cc between stations, which would also imply an increase in the scale distance (r). A rainfall pattern at one station frequently becomes the pattern later in the day at a station east of the first station.

To examine the impact of duration on the results, a more laborious project was undertaken with the hourly data. Offhand the data base and data handling would seem to be 24 times as great, but since the number of no-rain cases is proportionately greater among the 1-hr statistics, the work was still manageable with undergraduate help from Regis College, Weston, MA.

The Hourly Precipitation Data were surveyed for the frequency of the maximum one-hour precipitation for all 24 hours of the day, disregarding any diurnal cycle that might exist in the New England rainfall. The results for the four successively larger areas (Table 3) are shown in Table 7. The unconditional cumulative frequencies (P_o) were obtained from the frequencies at five widely scattered stations (Boston, MA; Burlington, Vermont; Caribou, Maine; Hartford, Conn.; Pittsfield, MA) that had complete records and were considered "typical" of the New England rainfall patterns. The values of z were obtained up to the cumulative frequency of 9.91 mm, making m(a) = 14. The resulting estimate of the scale distance, for New England January 1-hr precipitation was $\hat{r}$ = 5.02 km. This value inserted in (29) and (24) would give a cc between the precipitation at Hartford, Conn. and Portland, Maine, distance s' = 286 km apart, the value of $\rho(s')$ = 0.45. By the tetrachoric method for dichotomously classified hourly rainfall the cc varied between 0.31 and 0.72 with an arithmetic average of 0.58. Again Model B tended to underestimate the cc, but provided a proper order of magnitude.

(4) New England July 1-hr Rainfall

The exercises on 24-hr rainfall supported a preconception that the rainfall patterns are more widespread and hence more persistent horizontally in midwinter than in midsummer. The 24-hr scale distance was 9.45 km in January compared with 5.19 km in July. To see if the same is true with the shorter duration in rainfall, the exercise on hourly rainfall in New England was repeated using July records for the same 21 years (1952-1972), again disregarding any diurnal cycle (which probably does exist in summer). The results are shown in Table 8. But because intensive rainfall is much more frequent in summer than in winter, the values of z were obtained up to the cumulative frequency of 27.7 mm, making m(a) = 21. The resulting estimate of the scale distance for New England July 1-hr rainfall was $\hat{r}$ = 3.61 km which again supports the view that the horizontal pattern is less persistent in summer than in winter. But, winter or summer, 1-hr rainfall patterns are expectedly less widespread than the 24-hr patterns, as revealed by the parameter sizes.

7.3 Example 3: PPI-Scope Radar Statistics

It is desirable to work on synoptic situations that essentially eliminate time as a factor, so that the study can be made of the modelling of strictly spatial variability. This is close to being accomplished with radar pictures, now routinely taken

Table 7. Summary of the Cumulative Relative Frequencies and the Resulting Values of z (Model B) of New England January 1-hr Precipitation in 21 Years (1952-1972). Areas 1 to 4 are defined in Table 3; the symbols are defined in the text

Amt (mm)	All Stations (P_o)	Area 1		Area 2		Area 3		Area 4	
		P_a	z	P_a	z	P_a	z	P_a	z
None or T	0.892	0.738	4.05	0.712	4.50	0.547	5.46	0.503	5.71
0.2	0.9371	0.797	4.55	0.777	4.83	0.655	5.56	0.608	5.79
0.5	0.9590	0.837	4.60	0.819	4.83	0.735	5.52	0.692	5.79
0.8	0.9708	0.864	4.84	0.846	5.09	0.783	5.65	0.748	5.86
1.0	0.9781	0.884	4.96	0.866	5.25	0.816	5.80	0.785	6.00
1.3	0.9840	0.9023	4.95	0.887	5.36	0.847	5.80	0.821	6.00
1.5	0.9874	0.9129	5.00	0.897	5.45	0.862	5.81	0.840	6.01
1.8	0.9902	0.9219	5.21	0.9065	5.61	0.876	5.97	0.855	6.17
2.0	0.9923	0.9317	5.27	0.9162	5.75	0.890	6.10	0.873	6.25
2.3	0.9936	0.9378	5.45	0.9236	5.80	0.899	6.13	0.882	6.30
3.6	0.9978	0.9737	5.50	0.9660	5.70	0.9552	6.04	0.9466	6.20
4.8	0.9990	0.9858	5.45	0.9805	5.87	0.9733	6.12	0.9700	6.30
7.4	0.9997	0.9959	5.39	0.9938	5.82	0.9917	6.05	0.9904	6.25
9.9	0.9999	0.9980	5.35	0.9971	5.83	0.9963	6.05	0.9958	6.14
s'(a)		146.1 km		193.5 km		293.9 km		415.1 km	
m(a)		14		14		14		14	
$\bar{z}$		5.04		5.41		5.86		6.06	
$\hat{s}$(a)		32.93		42.52		58.08		66.49	
$\hat{r}$(a)		4.44 km		4.56 km		5.06 km		6.24 km	

Table 8. Summary of Cumulative Relative Frequencies and the Resulting Values of z (Model B) of New England July 1-hr Rainfall in 21 years (1952-1972). Areas 1 to 4 are defined in Table 3. The symbols are defined in the text

Amt (mm)	All Stations (P_o)	Area 1		Area 2		Area 3		Area 4	
		P_a	z	P_a	z	P_a	z	P_a	z
None or T	0.9504	0.782	4.98	0.734	5.40	0.561	6.22	0.493	6.50
0.25	0.9644	0.819	4.96	0.776	5.32	0.614	6.21	0.550	6.50
0.50	0.9719	0.841	5.06	0.798	5.50	0.650	6.37	0.591	6.60
0.8	0.9767	0.856	5.32	0.816	5.60	0.680	6.38	0.625	6.62
1.0	0.9792	0.866	5.35	0.826	5.63	0.701	6.43	0.649	6.68
1.3	0.9827	0.879	5.27	0.840	5.60	0.727	6.50	0.678	6.69
1.5	0.9842	0.886	5.30	0.848	5.68	0.738	6.55	0.691	6.76
1.8	0.9861	0.893	5.37	0.855	5.72	0.748	6.53	0.705	6.74
2.0	0.9872	0.898	5.41	0.860	5.77	0.759	6.59	0.715	6.81
2.3	0.9880	0.9012	5.40	0.864	5.85	0.766	6.60	0.726	6.77
3.6	0.9920	0.9286	5.38	0.895	5.85	0.818	6.55	0.736	6.75
5.0	0.9940	0.9428	5.40	0.9124	6.00	0.847	6.61	0.822	6.80
7.5	0.9964	0.9634	5.30	0.9395	5.91	0.893	6.52	0.875	6.70
9.9	0.9977	0.9759	5.30	0.9577	5.95	0.9250	6.52	0.9130	6.70
12.4	0.9984	0.9835	5.35	0.9694	6.02	0.9464	6.60	0.9382	6.70
15.0	0.9991	0.9886	5.25	0.9778	6.00	0.9598	6.61	0.9540	6.75
17.5	0.9994	0.9922	5.25	0.9838	6.01	0.9717	6.60	0.9677	6.70
20.1	0.9996	0.9944	5.27	0.9883	6.01	0.9795	6.61	0.9756	6.80
22.6	0.9997	0.9961	5.27	0.9919	6.06	0.9850	6.61	0.9822	6.80
25.3	0.99974	0.9972	5.06	0.9942	5.75	0.9894	6.41	0.9872	6.65
27.7	0.99984	0.9979	5.25	0.9955	6.05	0.9920	6.55	0.9908	6.72
m(a)		21		21		21		21	
$\bar{z}$		5.26		5.79		6.50		6.70	
s(a)		38.37		55.49		90.72		104.11	
r(a)		3.81 km		3.48 km		3.24 km		3.98 km	

by the National Weather Service. Radar scans the Precipitation within a radius of 125 nmi or 250 nmi in a matter of seconds.

A typical picture of a radar-scope survey of the precipitation surrounding a station shows echoes that look like white clouds on a black background (for example, the negative of Figure 23); such pictures permit an examiner to judge the direction and distance of storms from the station. Time changes give the direction and speed of movement, making the radar primarily a tool of short-range forecasting. But pictures taken regularly at many stations in the United States, for six years or more, provide a basis for a climatological study of the areal extent of precipitation. The results of such a study are reviewed and interpreted below.

The outer circle in Figure 23 has a radius of 125 nmi, the innermost circle has a radius of 25 nmi, and the second last circle has a radius of 100 nmi. Between the 25 nmi and 100 nmi circles, the area of 29452 nmi^2 is divided into 64 cells, each 460 nmi^2. Two adjacent cells of the innermost ring have twice the single-cell area, four cells have four times the single-cell area, the whole inner ring has eight times the single-cell, two rings have 16 times the area, three rings have 32 times the basic area, and, lastly, the whole usable space has 64 times the basic area. This made it possible to study the frequency with which fractions of an area were covered by precipitation echoes, as a function of areal size. This was done at five widely scattered stations within contiguous United States for the four midseason months, using eight observations per day at 3-hr intervals. Six years of radar-picture records were used (1969-1974). At each station, in each month, therefore, there were a total of 1440 or 1488 radar pictures surveyed. On the average, there were less than 119 missing pictures per month per station.

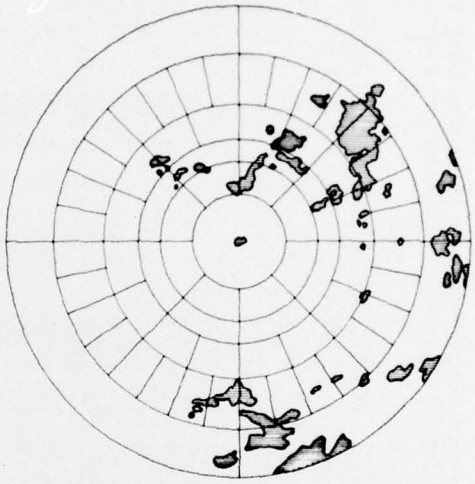

Figure 23. Sample of a PPI Radar-Scope Picture of Storms Within 125 nmi of the Radar Station. The area between the circles of radii 25 nmi and 100 nmi has been divided into 64 cells, each of 460 nmi^2

As an example, Table 9 shows the cumulative relative frequency of the fractional coverage of each area from one cell (460 nmi^2) to all cells or rings (29, 452 nmi^2). The kind of information in Table 9 is ready for entry in Figures 9 and 11 through 19. The frequencies of the first line, for 10/10 coverage, are used

Table 9. The Cumulative Relative Frequency of Each Fractional Coverage of Areas of Increasing Size by Radar Echoes. The example is for Cape Hatteras, NC July, based on 6 years (1969-1974) of radar pictures taken at 3-hr intervals. The single-point relative frequency of a radar echo is 0.04

Area (nmi^2) / Fractional Cover	460	920	1841	3682	7363	14726	29452
10/10	0.0045	0.0011	negl	negl	negl	negl	negl
9/10	0.0084	0.0035	0.0003	negl	negl	negl	negl
8/10	0.012	0.0067	0.0020	0.0005	negl	negl	negl
7/10	0.016	0.0097	0.0039	0.0013	0.0005	negl	negl
6/10	0.021	0.0159	0.0080	0.0046	0.0013	0.0005	negl
5/10	0.025	0.0211	0.0128	0.0062	0.0037	0.0029	negl
4/10	0.034	0.028	0.023	0.0137	0.0102	0.0062	0.0021
3/10	0.054	0.039	0.037	0.026	0.023	0.016	0.0103
2/10	0.085	0.062	0.059	0.055	0.052	0.047	0.040
1/10	0.113	0.115	0.109	0.117	0.119	0.130	0.136

with Figure 9, those on the second line for 9/10 coverage are used with Figure 19, ···, those on the line for 1/10 coverage are used with Figure 11.

Since the single-point frequency of a radar echo was 0.04 (Table 9), the cumulative relative frequency, $P_o = 0.96$, was entered on the left-hand side of Figure 9 and the interpolated curve was followed till the value $P_f = (1-0.0045)$ was reached. (The reading 0.0045 is on the right-hand scale.) The abscissa showed a value of $z = 4.20$. Likewise a z-value was found for each pair of values of P_o and P_f (Table 10), ultimately leading to the geometric mean value of the scale distance, $\hat{r} = 0.79$ nmi or 1.46 km. (The z-values were not read, or recorded, in instances when the curves in Figures 11 through 19 were too flat for a reliable reading.)

Once the scale distance is determined, or assigned a value, it can be used with Figures 9 and 11 through 19 in a reverse procedure to estimate the probability of fractional cover, by precipitation, or areas of varying size. Using the value $r = 0.79$ nmi, this was done for Cape Hatteras, July rainfall, whose single-point probability is 0.04. The resulting estimates are shown (Table 11) to compare with the 6-year sample frequencies (Table 9).

For the four midseason months at five stations the estimates of scale distance (r) were as shown (Table 12), together with geometric means by station and by month. Table 12 shows large variations in the estimate of scale distance, which make it difficult to associate its magnitude with geography or climatic regime. There may be a lesser horizontal persistence at Key West, Florida, at a latitude lower than 25^{o}N, compared with that at other stations, all of which are above 35^{o}N. But this apparent difference could be due to sampling errors and noise in the radarscope data.

There is a reasonable variation with season of the year. The horizontal persistence or the scale of weather patterns should be greater in winter than in summer, and this is reflected in the relative sizes of the mean scale distance: 3.63 km in January versus 1.48 km in July.

Making $r = 1.48$ km as the universal scale distance in July at all seasons, estimates were made of the probability of each fractional coverage by radar echoes at each of the five stations in the sample, to compare with the corresponding 6-year sample frequencies. The overall rms difference was 0.0067, which is less than 1 percent in the probability of areal coverage. But the rms difference varies systematically from a low of 0.12 percent in the probability of full coverage to a high of 1.2 percent in the probability of 1/10 areal coverage. Figure 24 shows graphically the difference between the Model B estimates of the probabilities of 3/10 areal coverage and the sample frequencies (marked by the x's) at Key West where the single-point probability is 0.02 and at Cape Hatteras, North Carolina where the single-point probability is 0.04. The model estimates of probability

Table 10. The Results for z by Entering the Data of Table 9 into the Graphs of Figures 9 and 11 to 19

s' Fractional Cover	21.45 nmi	30.34	42.90	60.68	85.81	121.35	171.62 nmi
10/10	4.20	5.06					
9/10	4.20	5.20	6.33				
8/10	4.30	5.18	6.08	6.50			
7/10	4.57	5.36	6.06	6.50	6.77		
6/10	4.55	5.25	5.96	6.35	6.86	7.29	
5/10	4.70	5.21	6.05	6.10	6.84	7.11	
4/10		5.45	5.84	6.50	6.68	7.18	7.58
3/10			5.86	6.58	6.70	7.20	7.45
2/10				6.40	6.53	7.40	7.50
1/10							
$\bar{z}$	4.42	5.24	6.03	6.42	6.73	7.24	7.51
s	21.42	37.90	65.15	85.54	106.15	150.75	182.28
r	1.00	0.80	0.66	0.71	0.81	0.80	0.94

Table 11. The Model B Estimates of the Probabilities of Each Fractional Coverage, from 10/10 to 1/10, by Precipitation, when the Single-Point Probability Is 0.04 and the Scale Distance Is 0.79 nmi. These probabilities, when compared with the frequencies in Table 1, show an rms difference of 0.0064 and a negative bias of 0.0013

Area (nmi^2)	460	920	1841	3682	7363	14726	29452
Fractional Cover							
10/10	0.0023	0.0010	0.0002	negl	negl	negl	negl
9/10	0.0067	0.0045	0.0020	0.0006	negl	negl	negl
8/10	0.012	0.0085	0.0047	0.0016	0.0003	negl	negl
7/10	0.018	0.014	0.0085	0.0036	0.00085	0.00011	negl
6/10	0.022	0.019	0.014	0.0077	0.0030	0.00050	negl
5/10	0.029	0.025	0.019	0.013	0.0070	0.0015	0.0001
4/10	0.039	0.037	0.031	0.022	0.013	0.0052	0.0009
3/10	0.052	0.050	0.047	0.039	0.029	0.015	0.0050
2/10	0.070	0.070	0.067	0.065	0.060	0.045	0.024
1/10	0.100	0.105	0.110	0.120	0.120	0.120	0.119

Table 12. The Sample Estimates of Scale Distance (r) for Each of Five Stations in the Four Midseason Months

Station	January (nmi)	April (nmi)	July (nmi)	October (nmi)	Annual Geometric Mean (nmi)	km
Minneapolis, MN	1.42	1.25	1.31	1.60	1.39	2.57
Key West, FL	1.54	1.33	0.47	0.81	0.94	1.74
Wichita, KS	2.72	1.59	0.87	1.32	1.49	2.75
Cape Hatteras, NC	2.41	1.69	0.79	0.84	1.28	2.37
Evansville, IN	2.01	1.45	0.76	1.96	1.44	2.67
5-Station Geometric Mean (nmi)	1.96	1.45	0.80	1.23	1.29	
Geometric Mean (km)	3.63	2.69	1.48	2.28		2.39

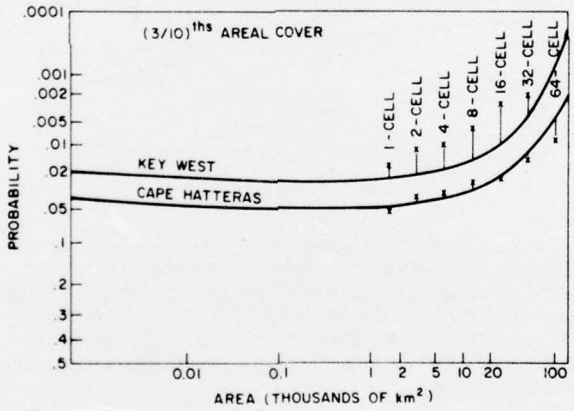

Figure 24. An Adaptation of Figure 13 to Show the Estimates of Probability (solid curves) of 3/10 Areal Coverage, by Echo-Producing Rainfall in July in the Vicinity of Key West, Florida and Cape Hatteras, North Carolina. The horizontal scale has been converted to area (km^2). The X's are the six-year sample estimates to compare with the model estimates

could well be favored over the noisy sample estimates. Model B implies that the Key West sample of six Julys underestimates the probability of 3/10 areal coverage by 1 percent or less for all areas from 1000 km^2 to 50,000 km^2.

The model extension of the above results is illustrated further in Figure 25. If the single-point frequency is 0.07, then Model B estimates no probability higher than 25 percent for 1/10 of an areal coverage. When the scale distance is 1.48 km, this probability is highest for an area of 100,000 km^2. For greater areas it will decrease eventually to zero.

Again, if the single-point probability is 25 percent, then the probability of 1/10 of an areal coverage will logically increase continucusly with the size of the area. But Model B specifies this probability as exceeding 50 percent in an area exceeding 5000 km^2.

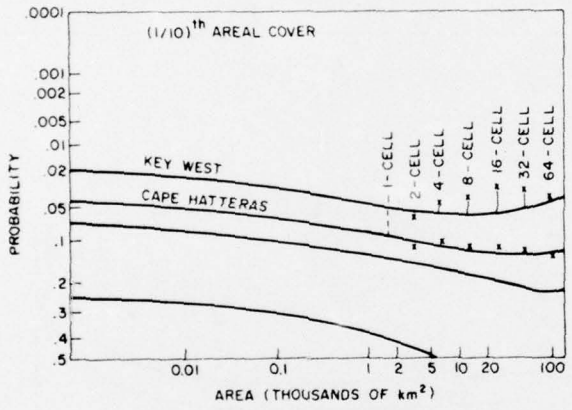

Figure 25. An Adaptation of Figure 11 to Show the Estimates of Probability (solid curves) of 1/10 Areal Coverage by Echo-Producing Rainfall in July When the Single-Point Probability is 0.02, 0.04, 0.07, or 0.25. The X's are the six-year sample estimates at Key West, Florida and Cape Hatteras, North Carolina

8. SUMMARY AND CONCLUSIONS

The stochastic models described in this paper and the resulting applications (primarily in Figures 6 through 9, 11 through 19) have been demonstrated on several practical problems in the areal extent of weather conditions or events. Two models were developed: Model A preferred for macroscale events and Model B for mesoscale events. Their limited success is a strong recommendation for further

efforts at improved modelling. There is the compelling realization that the above results have been dependent on Monte Carlo simulation. The challenge remains to solve the problem analytically, to present the probabilities through algorithmic equations that could be used in computer programming, as was done for the duration of n-day precipitation by Todorovic and Woolhiser.[12]

Compared with the direct estimates of cc, Model A has overestimated the horizontal persistence of 100-mb temperatures over long distances, while Model B has underestimated, somewhat, the horizontal persistence of surface precipitation. But, for the intended purpose of estimating the probability of a full or fractional areal coverage, the models demonstrate a workable simplicity, requiring a single parameter (r) for each season but apparently not for each geographic regime.

The parameter of Model B that measures the horizontal persistence and is termed the scale distance (r) shows a logical decrease, in wintertime, from 9.45 km for 24-hr precipitation to 5.02 km for 1-hr precipitation to 3.63 km for the "instantaneous" precipitation rate of radar echoes. Likewise, in summertime the scale distance has decreased from 5.19 km for 24-hr precipitation to 3.61 km for 1-hr precipitation to 1.48 km for an "instantaneous" rate.

When the scale distance, r(km), is known, Figures 6 through 9, 11 through 19 give the desired probability estimates to correspond to a given single-point probability. At a selected value of z on the horizontal scale the corresponding area, $s'^2(km^2)$, is obtained from

$$s' = r \cdot 2^z \quad .$$

If the area is given as s'^2, or a line of travel is given as s', then the z-value for entry into Figures 6 through 9 and 11 through 19 is given by

$$z = (\ell n\, s' - \ell n\, r)/\ell n\, 2 \quad .$$

12. Todorovic, P. and Woolhiser, D.A. (1975) A stochastic model of N-day precipitation, J. Appl. Meteorol., 14:17-24.

References

1. Riedel, J.F., Appleby, J.F., and Schloemer, R.W. (1956) Seasonal Variation of the Probable Maximum Precipitation East of the 105th Meridian for Areas from 10 to 1000 sq. miles and Durations of 6, 12, 24, and 48 Hours, U.S. Dept. of Commerce, Hydrometeorological Report No. 33, Washington, D.C.
2. Court, A. (1961) Area-point rainfall formulas, J. Geophys. Res., 66:1823-1831.
3. Briggs, J. (1972) Probability of aircraft encounters with heavy rain, Meteorol. Mag., 101:8-13.
4. Roberts, C.F. (1971) A note of the derivation of a scale measure for precipitation events, Monthly Weather Review, 99:873-876.
5. Sims, A.L. and Jones, D.M.A. (1975) Frequencies of short-period rainfall rates along lines, J. Appl. Meteorol., 14:170-174.
6. Stroud, A.H. and Secrest, D. (1966) Gaussian Quadratic Formulas, Prentice-Hall, Englewood Cliffs, New Jersey.
7. Blom, Gunnar (1958) Statistical Estimates and Transformed Beta-Variables, John Wiley and Sons, New York.
8. Gringorten, I.I. and Tattelman, P. (1970) Point and Route Temperatures for Supersonic Aircraft, AFSG, No. 233, AFCRL-70-0420, Bedford, MA.
9. Bertoni, E.A. and Lund, I.A. (1964) Winter Space Correlations of Pressure, Temperature and Density to 16 km, ERP, No. 75, AFCRL-64-1020, Bedford, MA.
10. National Bureau of Standards (1959) Table of the Bivariate Normal Distribution Function and Related Functions, NBS Appl. Math. Series, No. 50, Govt. Printing Office, Washington, D.C.
11. Gringorten, I.I. (1971) Modelling conditional probability, J. Appl. Meteorol., 10:646-657.
12. Todorovic, P. and Woolhiser, D.A. (1972) A stochastic model of N-day precipitation, J. Appl. Meteorol., 14:17-24.